Final Report

A Unified Approach to Concrete Mix Design Optimization for Durability Enhancement and Life-Cycle Cost Optimization

(Contract Number BC 380)

submitted to

Florida Department of Transportation Research Center
605 Suwannee Street
MS 30
Tallahassee, Florida 32399

submitted by

William H. Hartt, Jingak Nam, and Lianfang Li
Center for Marine Materials
Department of Ocean Engineering
Florida Atlantic University – Sea Tech Campus
101 North Beach Road
Dania Beach, FL 33004

October 16, 2002

EXECUTIVE SUMMARY

Concrete bridges in coastal locations, as are common in Florida, are susceptible to chloride induced reinforcing steel corrosion and to resultant concrete cracking and spalling. Design approaches adapted in the past decade by the Florida Department of Transportation to provide enhanced corrosion resistance include 1) use of high performance concretes; that is, ones with a) low water-to-cement ratio and b) pozzolanic and corrosion inhibiting admixtures, 2) 76 mm (3.0 in) and 102 mm (4.0 in) of cover over reinforcement for prestressed and cast-in place concretes, respectively, and 3) elevation of substructure components above four meters (12 feet), where feasible. At the same time, Florida concretes, for the most part, are formulated using native aggregates, the coarse type of which is a relatively porous limestone (a more dense Alabama limestone may be employed in the panhandle region of the State). As such, basic principles suggest that the structure and properties of Florida coarse aggregates act against the overall objective of achieving 1) relatively impermeable concretes and 2) the requisite longevity for coastal bridges, which is now 75 years.

The present study was based upon prior micro-compositional analyses of cores taken from the upper splash zone region of the Long Key Bridge which showed that chlorides were located in the paste only and not in the coarse aggregate. Such a finding infers that the ingress path for this species (chlorides) circumvented coarse aggregate particles such that these aggregates were of benefit rather than being detrimental to durability enhancement. Accordingly, the possibility exists that mix designs could be formulated where, by optimized grading and blending of coarse and perhaps fine aggregates, enhanced diffusional path tortuosity and a reduced chloride ingress rate could be affected. The objective of the present study was to more comprehensively investigate the influence of native Florida limestone coarse aggregates in concrete upon chloride diffusion and, based upon the results, propose mix designs that focus specific attention upon aggregate properties such that corrosion related durability is enhanced.

To accomplish this objective, a series of mortar and concrete specimens were fabricated and, subsequent to curing, exposed to cyclic ponding with a ten w/o NaCl solution. After approximately one year, the exposures were terminated and chloride concentration was measured as a function of depth below the exposed surface by a wet chemistry method. From this, the effective diffusion coefficient was calculated. Mix design variables for the mortar specimens included 1) water-to-cement ratio (0.38, 0.45, and 0.55), 2) type of silica sand (two different

fineness moduli), and 3) sand-cement ratio. For the concrete specimens, all of which utilized silica sand of the higher fineness modulus, the variables were 1) water-to-cement ratio (0.38, 0.45, and 0.52), 2) coarse aggregate type (porous Florida limestone (Southdown), dense Alabama limestone (Vulcan), and Ohio quartz (Sidley)), 3) coarse aggregate-fine aggregate-cement ratio, and 4) coarse aggregate grading (as-received, which did not conform to AASHTO M-43 (alternatively, ASTM C33) versus rescreened material that was regraded to within specification). It was intended that results from these exposures would allow, first, comparison of the native coarse aggregate with other products, including one has been reported to be particularly dense and impermeably (the Ohio quartz) and, second, determination of the affect of mix design upon chloride intrusion rate.

The results showed that the effective chloride diffusion coefficient, D_{eff}, and the surface chloride concentration, c_s, are both important parameters with regard to intrusion rate. Also, D_{eff} for concrete specimens fabricated using the porous Florida coarse aggregate was only 16 percent higher than with the Alabama limestone and 26 percent higher than with the Ohio quartz. Thus, the porous Florida limestone performed comparably with dense, impermeable aggregates from other regions of the country with regard to chloride ingress rate and corrosion related durability. Also, concrete specimens prepared using the coarse aggregate that was rescreened and regraded to within AASHTO M-43 (ASTM C33) specification had a lower D_{eff} than did those prepared using the as-received aggregate, although the difference may not be of practical significance. With further mix design refinements, it may be possible to affect additional D_{eff} reductions based upon aggregate grading modification alone. It is recommended that, first, a statistically significant determination be made of the fine and coarse aggregate gradings in concretes that are being delivered to FDOT bridge construction sites and, second, research continue in order to develop improved mix design formulations from the perspective of enhanced resistance to chloride intrusion and reinforcement corrosion.

TABLE OF CONTENTS

TABLE OF CONTENTS (continued)

LIST OF TABLES

LIST OF TABLES (CONTINUED)

LIST OF FIGURES

LIST OF FIGURES (continued)

LIST OF FIGURES (continued)

INTRODUCTION

Overview of Concrete and Concrete Deterioration Processes

General: While concrete has evolved to become the most widely used structural material in the world, the fact that its capacity for plastic deformation and, hence, its ability to absorb mechanically imparted energy is essentially nil imposes major practical service limitations. This shortcoming is most commonly overcome by incorporation of steel reinforcement into those locations in the concrete where tensile stresses are anticipated. Consequently, concerns regarding performance must not only focus upon properties of the concrete per se but also of the embedded steel and, in addition, the manner in which these two components interact. In this regard, steel and concrete are in most aspects mutually compatible, as exemplified by the fact that the coefficient of thermal expansion for each is approximately the same. Also, while boldly exposed steel corrodes actively in most natural environments at a rate that requires use of extrinsic corrosion control measures (for example, protective coatings for atmospheric exposures and cathodic protection in submerged and buried situations), the relatively high pH of concrete pore water (pH ≈ 13.0-13.8) promotes formation of a protective passive film such that corrosion rate is negligible and decades of relatively low maintenance result.

Corrosion Mechanism: Disruption of the passive film upon embedded reinforcement and onset of active corrosion can arise in conjunction with either of two causes: carbonation or chloride intrusion (or a combination of the two). In the former case (carbonation), atmospheric carbon dioxide (CO_2) reacts with pore water alkali according to the generalized reaction,

$$Ca(OH)_2 + CO_2 \rightarrow CaCO_3 + H_2O, \qquad (1$$

which consumes reserve alkalinity and reduces pore water pH to the 8-9 range, where steel is no longer passive. For dense, high quality concrete (for example, high cement factor, low water-cement ratio, and pozzolanic admixture) carbonation rates are typically on the order of one mm per decade or less; and so loss of passivity from this cause within a normal design life is not generally a concern. On the other hand, carbonation is often a problem for older structures; first, because of age per se and, second, because earlier generation concretes were typically of relatively poor quality (greater permeability) than more recent ones.

Chlorides, on the other hand, arise in conjunction with deicing activities upon northern roadways or from coastal exposure. While this species (Cl^-) has only a small influence on pore water pH per se, concentrations as low as 0.6 kg/m^3 (1.0 pcy) (concrete weight basis) have been projected to compromise steel passivity. In actuality, it is probably not the concentration of chlorides per se that governs loss of passivity but rather the ratio of chlorides to hydroxides ($[Cl^-]/[OH^-]$), since the latter species (OH^-) acts as an inhibitor. This has been demonstrated by aqueous solution experiments from which it is apparent that the Cl^- threshold for loss of steel passivity increased with increasing pH (1-6). On this basis, the relative amount of cement in the concrete mix and cement alkalinity are likely to affect the onset of corrosion. Considerable research effort has been focused upon identification of a chloride threshold; however, a unique value for this parameter has remained illusive, presumably because of the role of cement, concrete mix, environmental, potential, and reinforcement (composition and microstructure) variables that are influential (7). Because Cl^- and not carbonation induced loss of passivity is of primary concern for bridge structures, subsequent focus in this report is upon this cause of corrosion alone.

Once steel in concrete becomes active, either in conjunction with chlorides achieving the threshold concentration or pore solution pH reduction from carbonation at the embedded steel depth, then the classical anodic iron reaction,

$$Fe \rightarrow Fe^{+2} + 2e^-, \qquad (2$$

and cathodic oxygen reaction,

$$\frac{1}{2}O_2 + H_2O + 2e^- \rightarrow 2OH^-, \qquad (3$$

occur at an accelerated rate. Despite the normally high alkalinity of concrete, acidification may occur in the vicinity of anodic sites because of oxygen depletion and hydrolysis of ferrous ions. Thus,

$$Fe^{+2} + 2H_2O \rightarrow Fe(OH)_2 + 2H^+. \qquad (4$$

The product H^+ may be reduced and, along with O_2 reduction at more remote cathodic sites, further stimulate the anodic process. Irrespective of this, the net reaction is,

$$Fe + \frac{1}{2}O_2 + H_2O \rightarrow Fe^{+2} + 2OH^- \rightarrow Fe(OH)_2, \quad (5$$

and, upon further oxidation,

$$2Fe(OH)_2 + \frac{1}{2}O_2 + H_2O \rightarrow 2Fe(OH)_3, \quad (6$$

with,

$$2Fe(OH)_3 \rightarrow Fe_2O_3 + 3H_2O, \quad (7$$

as drying takes place.

Interestingly, corrosion per se is seldom the cause of failure in reinforced concrete components and structures. This arises because the final corrosion products (either ferric oxide or hydroxide) have a specific volume that is several times greater than that of the reactant steel; and their accumulation in the concrete pore space adjacent to anodic sites leads to development of tensile hoop stresses about the steel which, in combination with the relatively low tensile strength of concrete (typically 1-2 MPa), ultimately causes cracking and spalling.

Damage of this type has evolved to become a significant concern in the case of coastal bridge sub-structures in Florida. Figure 1 illustrates the deterioration process schematically where chlorides accumulate within the submerged zone from inward sea water migration and in the atmospheric zone as a consequence of capillary flow, splash, and spray. The lack of dissolved oxygen in the submerged zone precludes Reaction 2, and so corrosion is rarely a problem here. However, ready availability of both Cl^- in the splash zone and of O_2 at contiguous, more elevated locations results in this location (splash zone) being particularly susceptible to corrosion induced damage. Figure 2 shows a photograph of a marine bridge piling that illustrates this.

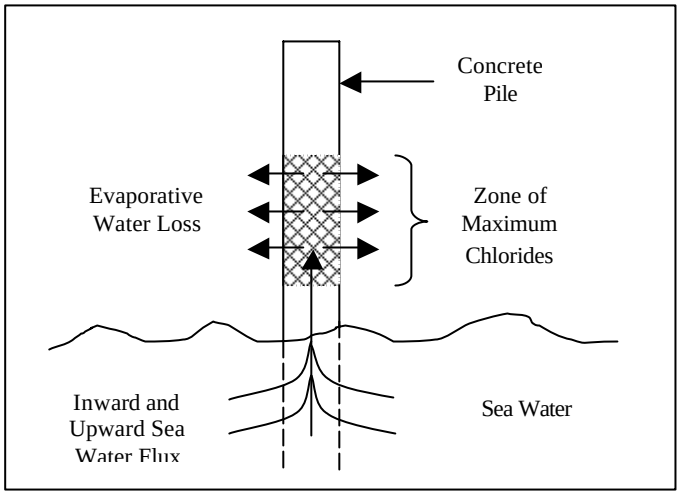

Figure 1: Schematic illustration of sea water migration and Cl^- accumulation within a marine piping.

Figure 2: Photograph of a cracked and spalled marine bridge piling.

Representation of Corrosion Induced Concrete Deterioration. Corrosion induced deterioration of reinforced concrete can be modeled in terms of three component steps: 1) time for corrosion initiation, 2) time, subsequent to corrosion initiation, for corrosion propagation (appearance of a crack on the external concrete surface), and 3) time for surface cracks to develop into spalls that

require repair, rehabilitation, or replacement. Figure 3 illustrates these schematically as a plot of cumulative damage versus time showing the above three components, T_i, T_p, and T_d (periods for initiation, propagation, continued damage (spalling), respectively) as well as the time-to-failure, T_f, or functional service life (modified from Tutti (8)). Of the former three terms, t_i typically occupies the longest period; and so it is upon this parameter that corrosion control measures generally focus. The approach adapted by the Florida Department of Transportation for new construction is to extend the time-to-corrosion initiation by a combination of 1) adequate concrete cover and 2) use of high performance concretes; that is, concretes with permeability reducing (pozzolanic) or corrosion inhibiting admixtures (or both). Likewise, the methods of Life-Cycle Cost Analysis or LCCA are employed to evaluate and compare different materials selection and design alternatives. This approach considers both initial cost and the projected life history of maintenance, repair, and rehabilitation costs that are required until the design life is reached. These are then evaluated in terms of the time value of money, from which Present Worth is determined. Comparisons between different options can then be made on a normalized basis. Figure 4 graphically illustrate an example life cycle cost scenario.

Analysis of Corrosion Initiation (Time-to-Corrosion). As noted above, the dominant component of the service life is normally T_i, the time in the case of Cl intrusion for this species to

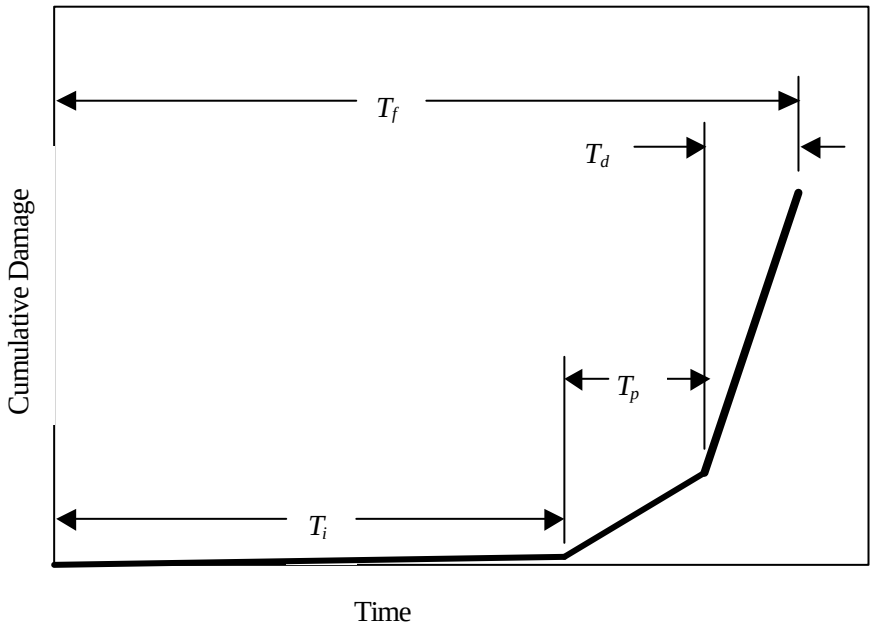

Figure 3: Schematic illustration of the various steps in deterioration of reinforced concrete due to chloride induced corrosion.

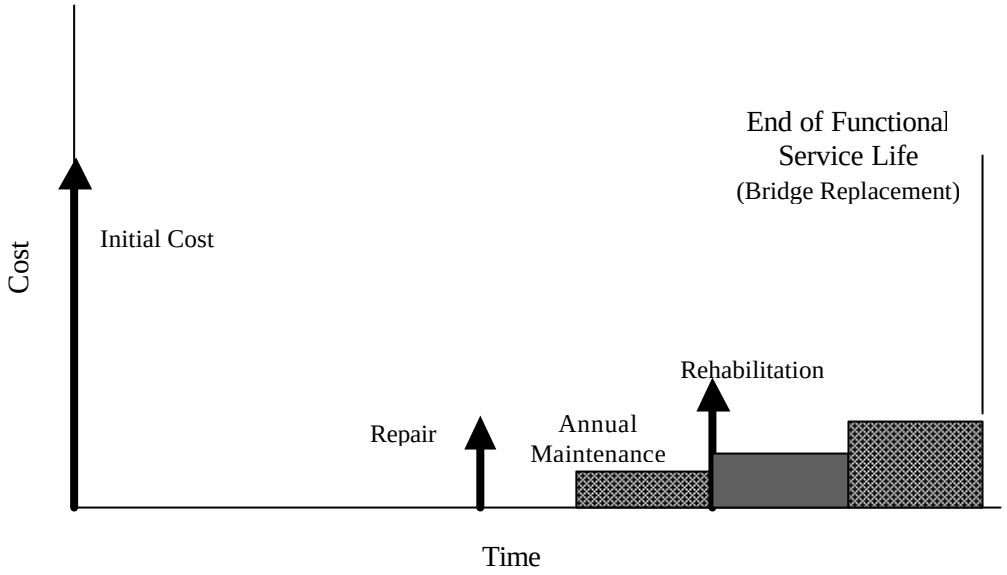

Figure 4: Schematic illustration of life cycle cost.

accumulate at the steel depth to the threshold concentration. The mechanism of this intrusion invariably involves both capillary suction and diffusion; however, for situations where the depth to which the former (capillary suction) occurs is relatively shallow compared to the reinforcement cover, diffusion alone is normally considered. Analysis of the latter (diffusion) is accomplished in terms of Fick's second law or,

$$\frac{\partial \mathbf{c}(\mathbf{x},\mathbf{t})}{\partial \mathbf{t}} = \frac{\partial}{\partial \mathbf{x}}\left(\mathbf{D}\cdot\frac{\partial \mathbf{c}(\mathbf{x},\mathbf{t})}{\partial \mathbf{x}}\right), \qquad (8$$

where $c(x,t)$ is the Cl^- concentration at depth x beneath the exposed surface after exposure time t and D is the diffusion coefficient. As Equation 8 is expressed, D is assumed to be independent of concentration. The solution in the one-dimensional case is,

$$\frac{c(x,t)-c_o}{c_s-c_o} = 1-\mathrm{erf}\left(\frac{x}{2\sqrt{D\cdot t}}\right), \qquad (9$$

where

c_o is the initial or background Cl^- concentration in the concrete, and

c_s is the Cl^- concentration on the exposed surface.

Assumptions involved in arriving at this solution are, first, c_s and D are constant with time and, second, the diffusion is "Fickian;" that is, there are no Cl^- sources or sinks in the concrete. In actuality, c_s increases with exposure time, although steady-state values generally in the range 0.3-0.7 (percent of concrete weight) have been projected to result after about six months (9). Factors that effect c_s have been projected to include type of exposure, mix design (cement content, in particular), and curing conditions (10). Also, the diffusion coefficient that is calculated from Equation 9 is termed an effective value, D_{eff}, since it is weighted over the relevant exposure period due, first, to the fact that c_s may vary and, second, because of progressive cement hydration. In addition, chemical and physical Cl^- binding invariably occur to some degree such that the concrete acts as a sink for this species and some fraction is no longer able to diffuse.

By the approach represented by Equation 9, $c(x,t)$, c_o, and c_s are measured experimentally (normally by wet chemistry analysis) and D_{eff} is calculated based upon knowledge of reinforcement cover and exposure time. Experimental scatter and error may be minimized by measuring $c(x,t)$ at multiple depths and employing a curve-fitting algorithm to calculate D_{eff}. Also, if D_{eff} is known from one sampling set, then c_{th}, the Cl^- threshold, can be determined by measuring $c(x,t)$ at the reinforcement depth (c_{rd}) at the time of corrosion initiation and solving Equation 9 recognizing that for this situation, $c_{rd} \approx c_{th}$. In any case, the parameters that affect Cl^- intrusion rate are c_s, and D_{eff}, where the former is exposure dependent and the latter a material property (actually, c_s is also sensitive to material composition and microstructure and D_{eff} is affected by exposure conditions (relative humidity and time-of-wetness, for example).

The approach of employing pozzolanic and corrosion inhibiting admixtures that has been adapted by the FDOT for enhancing concrete durability, as noted above, can be related to and interpreted in terms of Equation 9. In this regard, $Ca(NO_2)_2$, in effect, increases c_{th}, whereas pozzolans (fly ash, silica fume, and blast furnace slag) reduce D_{eff}. Surface $[Cl^-]$ may also be affected.

PROJECT BACKGROUND

Chloride Distribution in Concrete

Results of a preliminary investigation in which the distribution of Cl^- in and migration through concrete cores from several bridges, including the Long Key Bridge in District 6, were

measured serve as the basis for the present research project. In this case, the core was acquired from the pile cap (inverted) which was about one m above mean high tide. The analyses involved two procedures; first, wet chemistry analysis of 1) micro-drilled powder and 2) chipped particles, with the product being acquired from separate coarse aggregate and cement mortar areas and, second, energy dispersive x-ray analysis (EDX), also upon individual coarse aggregate and mortar areas. In both cases, the sample areas were on a fractured surface of the core at a given depth below the exposed surface. EDX analyses were also performed as a function of depth relative to this exposed surface. Table 1 presents the results from the wet chemistry analyses and Table 2 for the EDX for the case of analyses at a particular depth. These indicate that the mortar-to-aggregate chloride concentration ratio in the former case (wet chemistry analysis) was 9:1 and in the latter (EDX analyses) 9.8. Figure 5, on the other hand, plots chloride concentration, [Cl], versus distance into the concrete beneath the exposed surface, as determined by EDX. This also indicates that, for any given depth, approximately ten times more chloride existed in the mortar

Table 1: Chloride analysis results for mortar and aggregate samples acquired from a concrete core as determined by wet chemistry.

Location	Sampling Technique	Chloride Conc.,* pcy (ppm)
Mortar	Drilling	7,055 (23.5)
Aggregate	Drilling	781 (2.6)
Mortar	Chipping	5,733 (19.1)
Aggregate	Chipping	634 (2.1)

*Acid soluble determination.

Table 2: Chloride analysis results for mortar and aggregate areas of a concrete core as determined by energy dispersive x-ray analysis.

Sample Site Designation	Location Type	Chloride Concentration, a/o*
1	Aggregate	0.13
2	Aggregate	0
3	Aggregate	0
4	Aggregate	0.41
5	Aggregate	0.61
6	Paste	1.72
7	Paste	2.78

*a/o Atomic percent.

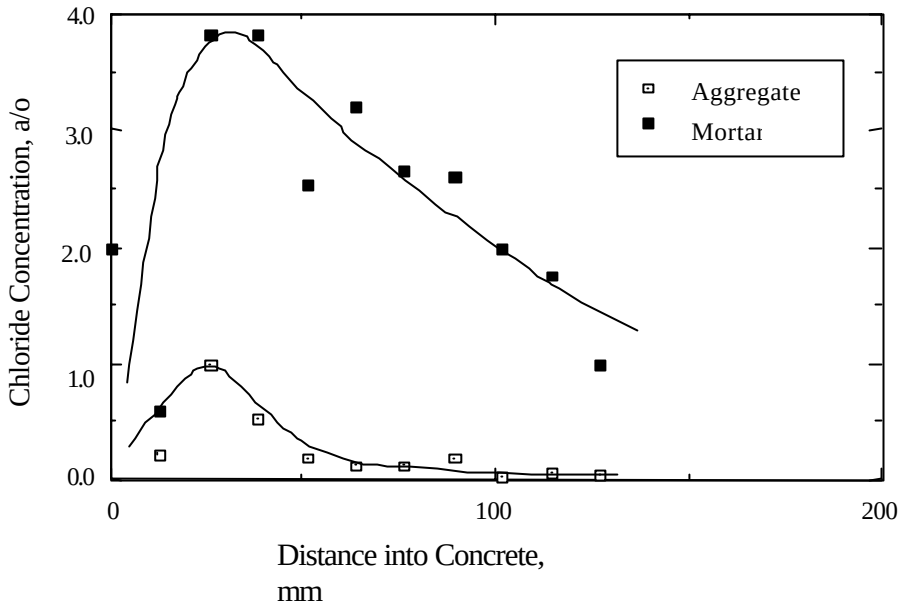

Figure 5: Chloride concentration as a function of depth for mortar and coarse aggregate areas of a concrete core.

compared to the aggregate. Thus, the mortar apparently provided the predominate inward migration path for the chlorides. Analyses upon cores from two other bridges confirmed this same trend. Ironically, this indicates that Florida limestone coarse aggregates, which have been criticized historically for their high porosity and low strength, apparently serve as obstacles to inward chloride migration and cause the diffusion path to be more tortuous than would otherwise be the case. The possibility exists also, although this was not been investigated, that fine aggregates as well as coarse ones serve as obstacles to inward chloride migration.

Mix Design Considerations

While ACI 211, "Standard Practice for Selecting Proportions for Normal, Heavyweight, and Mass Concrete," indicates that concrete mix design involves consideration of economic factors in perspective of placeability, strength, durability, density, and appearance, in practice mix proportioning is normally based upon the properties of local aggregates and attainment of the requisite strength at minimized unit cost. As such, corrosion related durability is typically enhanced by reducing the water-cement ratio or by inclusion of permeability reducing or corrosion inhibiting admixtures (or a combination of these) but with no consideration given to mix proportioning. In this regard, Table 3, which is also from ACI 211, provides an interrelationship guide between 1) nominal maximum size of coarse aggregate, 2) fineness

modulus of fine aggregate, and 3) coarse aggregate volume fraction to achieve an acceptable workability for concrete placement. This indicates that the maximum allowable volume fraction of coarse aggregate increases with increasing nominal maximum coarse aggregate size and with decreasing fine aggregate fineness modulus and extends over the range from 0.44 to 0.71 for a nominal maximum coarse aggregate size from 9.5 mm (3/8 in) to 25 mm (1 in), respectively. Thus, a range of aggregate proportioning is available to the concrete mix designer.

Table 3: Guide for achieving a fixed, acceptable degree of concrete workability as a function of maximum coarse aggregate size and fine aggregate fineness modulus.

Nominal Maximum Aggregate Size, mm (in.)	Volume of Oven-Dried-Rodded Coarse Aggregate per Unit Volume of Concrete			
	Fine Aggregate Fineness Modulus			
	2.40	2.60	2.80	3.00
9.5 (3/8)	0.50	0.48	0.46	0.44
12.7 (1/2)	0.59	0.57	0.55	0.53
19 (3/4)	0.66	0.64	0.62	0.60
25.4 (1)	0.71	0.69	0.67	0.65
38 (1 1/2)	0.75	0.73	0.71	0.69
50.8 (2)	0.78	0.76	0.74	0.72
76.2 (3)	0.82	0.80	0.78	0.76
152 (6)	0.87	0.85	0.83	0.81

PROJECT OBJECTIVE

The finding that chlorides in concrete apparently do not migrate through Florida limestone coarse aggregates but, instead, through the mortar (or paste alone) suggests that mix design protocols should take into account the proportioning of aggregates with durability, as well as with strength and economics (particularly if represented in a LCCA basis), in mind. This suggests that it should be possible to establish mix designs of the necessary strength but with optimized durability (due consideration must also be give to workability, density, and appearance). The results in Tables 1 and 2 and Figure 5 suggest that, by proper control of coarse aggregate proportioning and gradation, reduced Cl^- penetration rate and enhanced embedded steel corrosion resistance can be realized. The purpose of the present project was to design, perform, and analyze a series of experiments that would, first, confirm the above finding that coarse aggregates in concrete constitute an impediment to Cl^- diffusion and, second, determine the extent to which

this phenomenon, if confirmed, can be employed in concrete mix design to improve resistance to reinforcement corrosion.

EXPERIMENTAL PROCEDURE

Mortar Specimens

Non-reinforced cylindrical mortar specimens 152 mm high by 76 mm in diameter of three different water-to-cement ratios, w/c, (0.38, 0.45, and 0.55) with either "low" or "high" fineness modulus (FM) silica sand fine aggregate (FA), and Type II cement were cast. Both sand types were obtained bagged from a local retail supplier. For each w/c ratio, a sand-to-cement ratio of 0, 0.5, 1.0, and 2.0 was employed for a total of 24 different mix designs. Table 4 shows the mix design parameters for the low FM fine aggregate cylinders and Table 5 for the high. Three cylinders of each mix design were cast. Specimens were demolded after one day, placed in a 100 percent relative humidity chamber, and sprayed daily with deionized water during the first week thereafter. The low FM mortar mix with w/c = 0.38 and sand-cement ratio two was too stiff to place, and the paste only (no FA) with w/c = 0.38 and 0.45 developed cracks during curing and were not exposed.

Concrete Specimens

Non-reinforced concrete block specimens 12.7 cm wide by 12.7 cm high by 20 cm long were cast using ASTM Type II cement, silica sand with fineness modulus 2.94 (same material as for the mortar specimens in Table 4), and coarse aggregate (CA) from each of three different sources. These were Southdown porous limestone (Florida), Vulcan dense limestone (Alabama), and Sidley quartz (Ohio); and are subsequently identified as SLF, VLA, and QO, respectively. It was intended that these represent a relatively broad range of what is commercially available, where the first (SLF) should be typical of what is employed in Florida, the second (VLA) being a more dense material that may be employed in the Florida panhandle region, and the third (QO) representing an extreme with regard to denseness and impermeability (11). In each case, the coarse aggregate was obtained directly from the company in 55 gallon steel drums. Figure 6 shows a photograph of each of these three materials. Samples of each CA were characterized

Table 4: Material properties and mix design parameters for mortar specimens prepared using low FM silica sand as the FA.

Bulk specific gravity (SSD)		2.56										
Total moisture (%)		9.65										
Absorption capacity (%)		2.15										
Surface moisture (%)		7.5										
Fineness modules		2.47										
Designation	L38-2	L38-1	L38-H	L38-0	L45-2	L45-1	L45-H	L45-0	L55-2	L55-1	L55-H	L55-0
w/c	0.38	0.38	0.38	0.38	0.45	0.45	0.45	0.45	0.55	0.55	0.55	0.55
Water (kg)	152	152	152	152	180	180	180	180	220	220	220	220
Cement (kg)	400	400	400	400	400	400	400	400	400	400	400	400
Air (%)	1	1	1	1	1	1	1	1	1	1	1	1
Sand/cement ratio	2.0	1.0	0.5	0.0	2.0	1.0	0.5	0.0	2.0	1.0	0.5	0.0
Masonry F.A SSD (kg)	800	400	200	0	800	400	200	0	800	400	200	0
Total Volume (m^3)	0.595	0.437	0.358	0.279	0.623	0.465	0.386	0.307	0.663	0.505	0.426	0.347
Quantity for one m^3												
Water (kg)	256	348	425	545	289	387	466	586	332	436	517	634
Cement (kg)	673	916	1118	1434	642	861	1037	1303	604	792	939	1153
Fine aggr, SSD (kg)	1345	916	559	0	1285	861	518	0	1207	792	470	0
Fine aggr. wet (kg)	1446	984	601	0	1381	925	557	0	1298	852	505	0
Actual water	155	279	383	545	193	323	428	586	241	376	481	634
Total (kg/m^3)	2274	2180	2101	1979	2216	2108	2021	1889	2143	2021	1925	1787
Vol of 3 cylinders +10% =2.30 liters												
Actual Mix												
Water (g)	424.1*	640.3	906.3*	1248.9	441.8	739.8	1006.9*	1344.1	553.5	862.8	1127.6*	1453.4
Cement (g)	1542.1	2099.2	2562.1	3286.7	1472.7	1972.8	2376.2	2986.9	1383.8	1816.4	2153.0	2642.6
Fine aggr. wet (g)	3246.1*	2256.7	1348.3*	0.0	3166.4	2120.7	1250.5*	0.0	2975.2	1952.7	1133*	0.0
Cast Date	07/13/00	07/14/00	07/13/00	07/11/00	07/14/00	07/14/00	07/13/00	07/11/00	07/11/00	07/14/00	07/13/00	07/11/00

* Mix design modified according to a FA surface moisture of 7.4.

using the Iowa Pore Index test and mercury porosimetry, the former being performed by the Iowa DOT and the latter by Micromeritics, Inc. of Norcross, GA.

Table 5: Material properties and mix design parameters for mortar specimens prepared using high FM silica sand as the FA.

Bulk specific gravity (SSD)	2.600	2.536	2.536	2.536	2.536
Total moisture (%)	2.00	1.92	1.92	1.92	1.92
Absorption capacity(%)	0.14				
Surface moisture (%)	1.86	1.92	1.92	1.92	1.92
Fineness modules	2.94				
Designation	L38-2S	L38-1S	L38-HS	L45-2S	L55-2S
w/c	0.38	0.38	0.38	0.45	0.55
Water (kg)	152	152	152	180	220
Cement (Kg)	400	400	400	400	400
Air (%)	1	1	1	1	1
Sand/cement ratio	2.0	1.0	0.5	2.0	2.0
Masonry F.A SSD (kg)	800	400	200	800	800
Total Volume (m3)	0.590	0.438	0.359	0.626	0.666
Quantity for 1m3					
Water (kg)	258	347	424	288	331
Cement (kg)	678	913	1115	639	601
Masonry F.A SSD (kg)	1356	913	558	1279	1202
Masonry F.A wet (kg)	1382	930	568	1303	1225
Actual water	233	329	413	263	307
Total (kg/m3)	2292	2172	2097	2206	2133
Vol of 3 cylinders +10% (l)	2.3				
Actual Mix					
Water (g)	697.5	760.3	952.0	609.4	711.0
Cement (g)	2034.7	2099.1	2565.3	1470.6	1382.2
Masonry F.A wet (g)	4145.2	2136.4	1305.5	2993.5	2813.6
Cast Date	01/06/01	01/11/01	01/11/01	01/11/01	01/11/01

A portion of the as-received CA from each source was partitioned according to material retained upon individual sieve sizes 19.1 mm (3/4 in.), 12.7 mm (1/2 in.), 9.5 mm (3/8 in.), 4.75 mm (No. 4), and 2.36 (No. 8). The CA was then re-proportioned as indicated by Table 6 to achieve conformity with standard #7 CA (12). The resultant CA was termed "ideal" and was employed in casting some of the concrete specimens. The remainder of the specimens were cast using the as-received SLF CA (termed "regular"), subject to the material having passed a 12.7

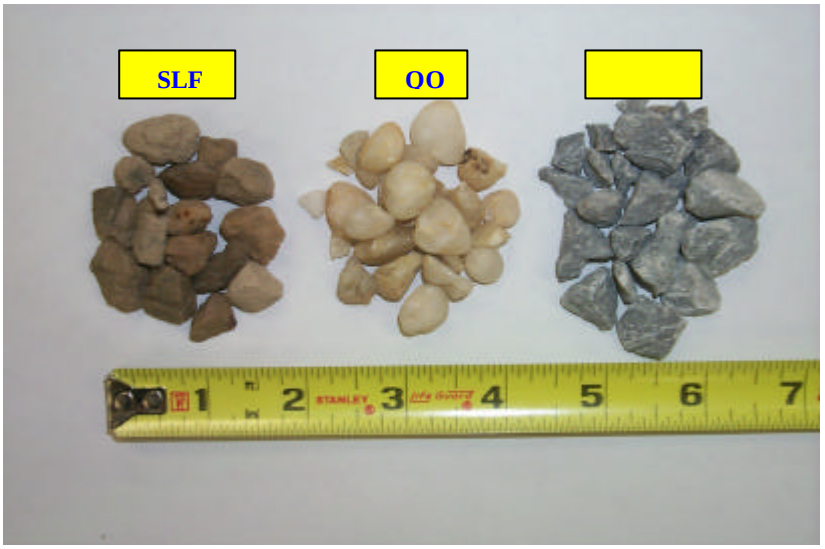

Figure 6: Photograph of the three CA types.

Table 6: Comparison of the present "ideal" CA proportioning with ASTM aggregate size #7.

	AASHTO #7, percent	Present Proportioning, percent
Pass 19 mm but retained on 12.7 mm	0-10	10
Pass 12.7 mm but retained on 9.5 mm	20-60	35
Pass 9.5 mm but retained on 4.75 mm (No. 4)	25-70	47
Pass 4.75 mm but retained on 2.36 mm (No. 8)	0-15	8
Retained on 2.36 mm	0-5	0

mm sieve. In addition to CA grading, mix design variables were 1) w/c (0.38, 0.45, and 0.52), 2) cement content (300, 400, and 500 kg/m^3), FA volume ratio (0.236 to 0.411), and 3) CA volume ratio (0.580 (normal), 0.464 (low), and 0.696 (high)). Table 7 gives the mix design for the "ideal" CA and Table 8 for the "regular." The proportioning of the high FM silica sand was also determined.

Exposure Testing

Approximately one week prior to the beginning of the exposures, specimens were removed from the humidity chamber and allowed to dry in laboratory air. An 18 cm by 10 cm plexiglass bath was then fasten to what had been the bottom 12.7 cm by 20 cm face (formed) of the concrete

Table 7: Aggregate properties and mix design for concrete specimens with "ideally" graded CA.

			SLF		
Aggregate Type	QO	VLA	S4	S8	S12
C.A. Bulk specific gravity (SSD)	2.62	2.73	2.45	2.45	2.45
C.A. Absorption capacity (%)	0.27	0.19	4.49	4.49	4.49
C.A. Moisture content (%)	0.05	0.02	0.83	0.83	0.83
C.A. OD Unit Weight (kg/m^3)	1462	1491	1415	1415	1415
F.A. Bulk specific gravity (SSD)	2.536	2.536	2.536	2.536	2.536
F.A. Total moisture (%)	1.02	1.02	1.02	1.02	1.02
F.A. Absorption capacity (%)	0.14	0.14	0.14	0.14	0.14
F.A. Surface moisture (%)	0.88	0.88	0.88	0.88	0.88
W/C	0.45	0.45	0.45	0.38	0.52
Cement content (kg)	400	400	400	400	400
Water, kg	180	180	180	152	208
Vol. Ratio of OD C.A	0.58	0.58	0.58	0.58	0.58
Coarse Aggregate SSD (kg)	850	866	858	858	858
Air content (m^3)	0.03	0.03	0.03	0.03	0.03
Vol of F.A (m^3)	0.338	0.346	0.313	0.341	0.285
Fine aggregate SSD (kg)	858	877	794	865	723
Fine aggregate (as-received–wet) (kg)	866	884	801	872	729
Extra water in F.A (kg)	8	8	7	8	6
Adjusted total water needed (kg)	172	172	173	144	202
Material for one m^3 of concrete (kg)					
water	172	172	173	144	202
cement	400	400	400	400	400
C.A. (SSD)	850	866	858	858	858
F.A. (as-received)	866	884	801	872	729
Total weight (kg/m^3)	2289	2323	2231	2274	2188
Material for each batch (kg)					
water	1.380	1.378	1.362	1.136	1.613
cement	3.200	3.200	3.148	3.148	3.200
C.A. (SSD)	6.802	6.931	6.749	6.749	6.860
F.A. (as-received)	6.928	7.074	6.302	6.866	5.833
Casting date	10/30/00	10/30/00	10/20/00	10/23/00	10/31/00

block specimens and a polyethylene pipe section was similarly attached around the bottom circumference of the mortar cylinders. These then became the upper face that was ponded during the exposures. In addition, the circumferential surface of the cylinders and side faces of the concrete block were coated with epoxy. Ponding commenced for the low FM mortar cylinders on December 14, 2000 (160-163 days after casting). Exposure of the high FM mortar cylinders began on June 14, 2001 (154-161 days after casting); and for the concrete blocks, SLF S1-S10 on

Table 8: Aggregate properties and mix design for concrete specimens with “regular” graded CA.

Mix Designation	S1	S2	S3	S9	S10	S5	S6	S7	S11
C.A. Bulk specific gravity (SSD)	2.45	2.45	2.45	2.45	2.45	2.45	2.45	2.45	2.45
C.A. Absorption capacity (%)	4.49	4.49	4.49	4.49	4.49	4.49	4.49	4.49	4.49
C.A. Moisture content (%)	0.83	0.83	0.83	0.83	0.83	0.83	0.83	0.83	0.83
C.A. OD unit weight (kg/m3)	1415	1415	1415	1415	1415	1415	1415	1415	1415
F.A. Bulk specific gravity (SSD)	2.536	2.536	2.536	2.536	2.536	2.536	2.536	2.536	2.536
F.A. Total moisture (%)	1.02	1.02	1.02	1.02	1.02	1.02	1.02	1.02	1.02
F.A. Absorption capacity (%)	0.14	0.14	0.14	0.14	0.14	0.14	0.14	0.14	0.14
F.A. Surface moisture (%)	0.88	0.88	0.88	0.88	0.88	0.88	0.88	0.88	0.88
Calculation for one m^3 of concrete									
W/C	0.45	0.45	0.45	0.45	0.45	0.38	0.38	0.38	0.52
Cement content (kg)	400	400	400	300	500	400	400	400	400
Water	180	180	180	135	225	152	152	152	208
Vol. ratio of OD C.A. to concrete	0.580	0.464	0.696	0.580	0.580	0.580	0.464	0.696	0.580
Coarse aggr. SSD (kg)	858	686	1029	858	858	858	686	1029	858
Air content (m^3)	0.03	0.03	0.03	0.03	0.03	0.03	0.03	0.03	0.03
Vol of F.A. (m^3)	0.313	0.383	0.243	0.390	0.236	0.341	0.411	0.271	0.285
Fine aggr. SSD (kg)	794	971	616	988	599	865	1042	687	723
Fine aggr. (as-received-wet) (kg)	801	980	622	997	604	872	1051	693	729
Extra water in F.A (kg)	7	9	5	9	5	8	9	6	6
Adjusted total water needed (kg)	173	171	175	126	220	144	143	146	202
Material for one m^3 of concrete									
Water (kg)	173	171	175	126	220	144	143	146	202
Cement (kg)	400	400	400	300	500	400	400	400	400
C.A. (SSD) (kg)	858	686	1029	858	858	858	686	1029	858
F.A. (as-received) (kg)	801	980	622	997	604	872	1051	693	729
Total weight kg/m^3	2231	2237	2225	2281	2182	2274	2280	2268	2188
Material for each batch of 7.87L	7.866	7.866	7.866	8.000	8.000	7.870	7.870	7.870	8.000
Water (kg)	1.362	1.349	1.374	1.010	1.758	1.136	1.124	1.149	1.613
Cement (kg)	3.148	3.148	3.148	2.400	4.000	3.148	3.148	3.148	3.200
C.A. (SSD) (kg)	6.749	5.399	8.099	6.860	6.860	6.749	5.399	8.099	6.860
F.A. (as-received) (kg)	6.302	7.711	4.892	7.977	4.835	6.866	8.275	5.456	5.833
Casting date	10/20/00	10/21/00	10/21/02	10/25/00	10/25/00	10/23/00	10/24/00	10/24/00	10/31/00

February 8, 2001 and S11, S12, VLA, and QO on February 22 of the same year (106-123 days after casting). The ponding solution was 10 w/o NaCl using a repetitive one week wet – one week dry cycle. All exposures were in air conditioned laboratory space. Figure 7 shows a

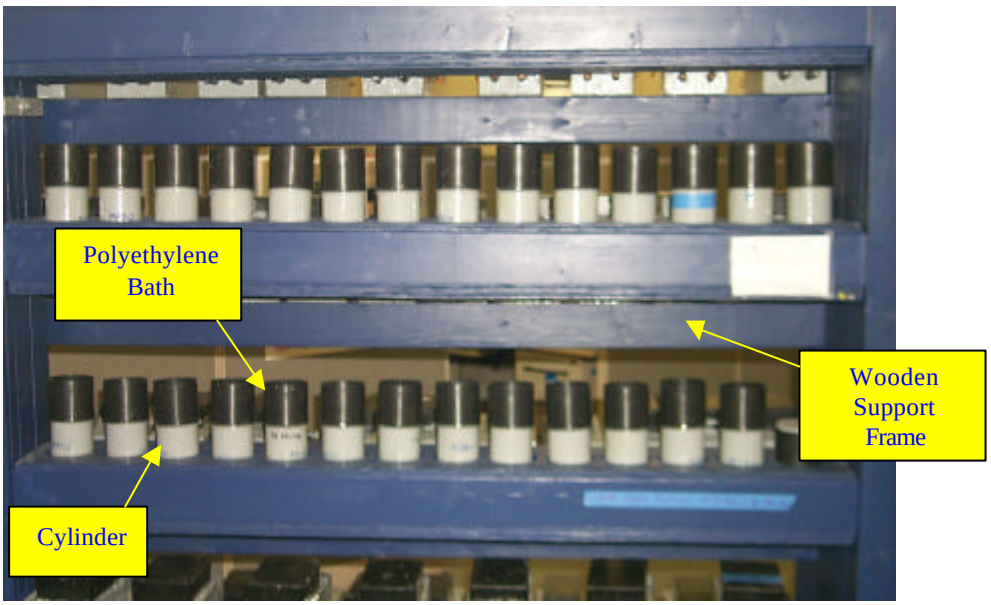

Figure 7: Photograph of mortar specimens under exposure testing.

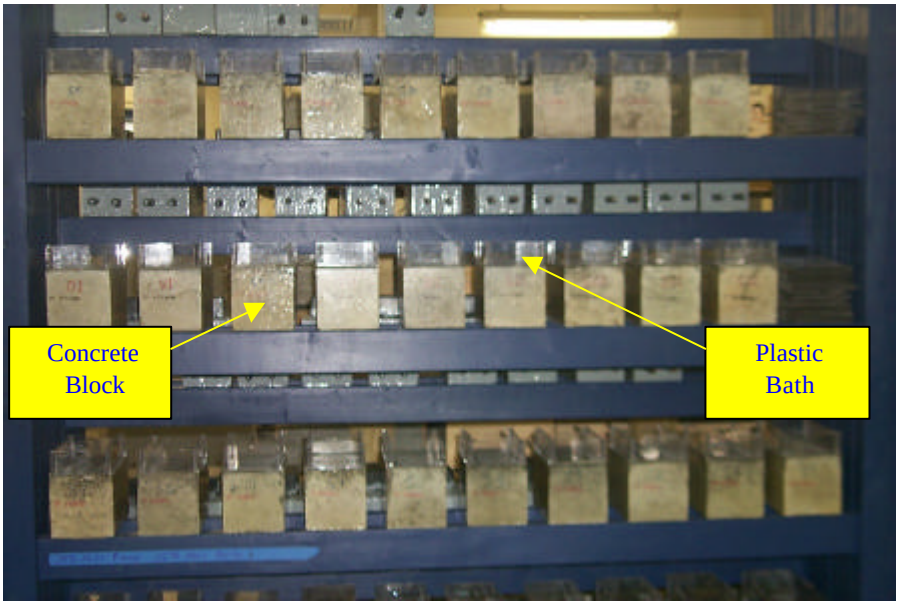

Figure 8: Photograph of concrete block specimens under exposure testing.

photograph of the mortar specimens under test and Figure 8 of the concrete.

Evaluation and Analysis

After the times indicated below, exposure of one of the three specimens of each mix design was terminated with the other two remaining under test. Exposure of the low FM mortar specimens was terminated on March 11, 2002 after 452 days exposure, the high FM silica sand ones on May 7, 2002 after 327 days, and the concrete blocks on April 17, 2002 after 433 days. Shortly thereafter, the specimens were analyzed for chloride concentration, [Cl^-], as a function of depth beneath the exposed surface. The protocol for the initial mortar specimen that was analyzed involved extracting a central 51 mm (nominal) diameter core along the cylinder axis from the exposed face. Both this and the remaining mortar ring were then sliced using a diamond blade and the slices analyzed. The purpose of this was to determine if [Cl^-] exhibited a radial variation as a consequence of either confinement at the outer surfaces, which should promote more rapid penetration at the specimen center, or ponding solution seepage at the epoxy-mortar interface, which would preferentially promote ingress at the periphery. The [Cl^-] difference between the two zones was determined not to be significant, as shown later; and so subsequent slicing involved the entire cylinder cross section. For the concrete blocks, a 51 mm diameter core was taken from the center of the ponded area and sliced the same as for the mortar specimens. In all cases, the slice closest to the exposed surface was three mm thick and subsequent ones six mm. The slices were broken into fragments, ground to powder using a Scienceware Micro-Mill, and analyzed for chlorides according to FDOT Test Method FM 5-516 (13). Values for c_s and D_{eff} were then calculated by fitting the [Cl^-] versus depth data using a least squares algorithm of Equation 9 and assuming c_o = 0. It was considered that the lack of specimen multiplicity was balanced by the fact that Cl^- analyses were performed as a function of depth with the magnitude of data scatter and material inhomogeniety being indicated by the extent to which the data conformed to or departed from the general trend.

RESULTS AND DISCUSSION

Silica Sand Sieve Analysis

Figure 9 shows the sieve analysis result for the high FM silica sand in comparison to the AASHTO/ASTM limits (12). This indicates that the particle size distribution was more narrow

than specified with insufficient material in the upper size range compared to the specified limits. Apparently, either the source material was graded improperly or it became segregated subsequently with the as-received material having been taken from a location in the stock where particle size was relative small.

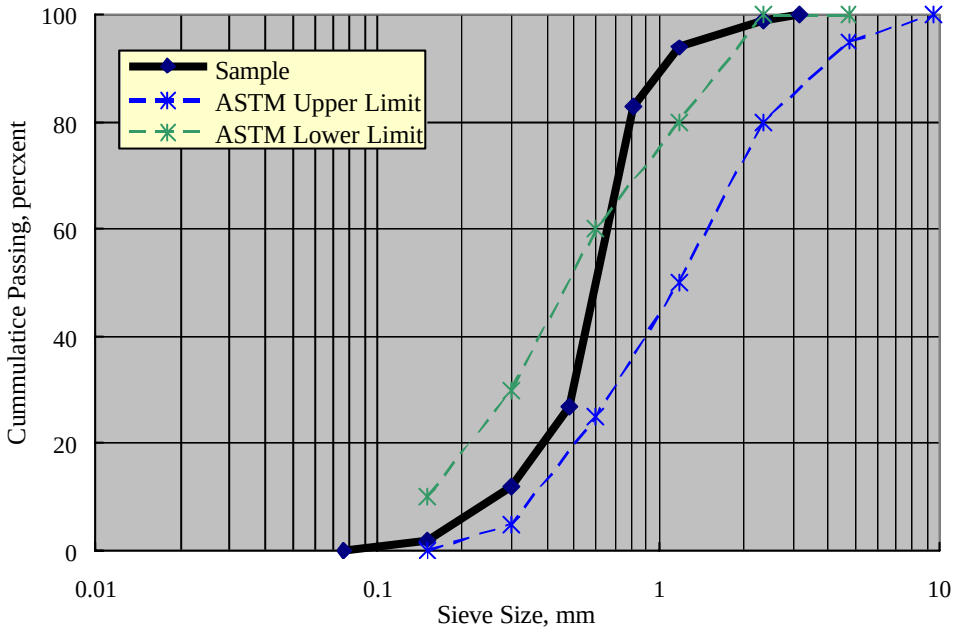

Figure 9: Grading curve for the high FM silica sand fine aggregate.

Coarse Aggregate Sieve Analysis

Similarly, Figure 10 shows the sieve analysis results for the as received (regular) and re-proportioned (ideal) CA, both in comparison to the AASHTO/ASTM upper and lower limit for #7 material (12). The #7 gradation was employed as the standard in lieu of #57 or #89 because the relatively small specimen size dictated that large aggregate particles be eliminated. The size of the re-proportioned ideal CA falls in the mid-range of the ASTM limit, as designed. The as-received material, on the other hand, corresponds to or exceeds the upper limit in the smaller particle size range; but this trend reverses at larger size. As for the fine aggregate (Figure 9), this is consistent with the CA size range being relatively narrow and the particles having segregated, either because of improper proportioning during processing or from handling thereafter.

The normal commercial CA processing and transportation method in Florida involves the

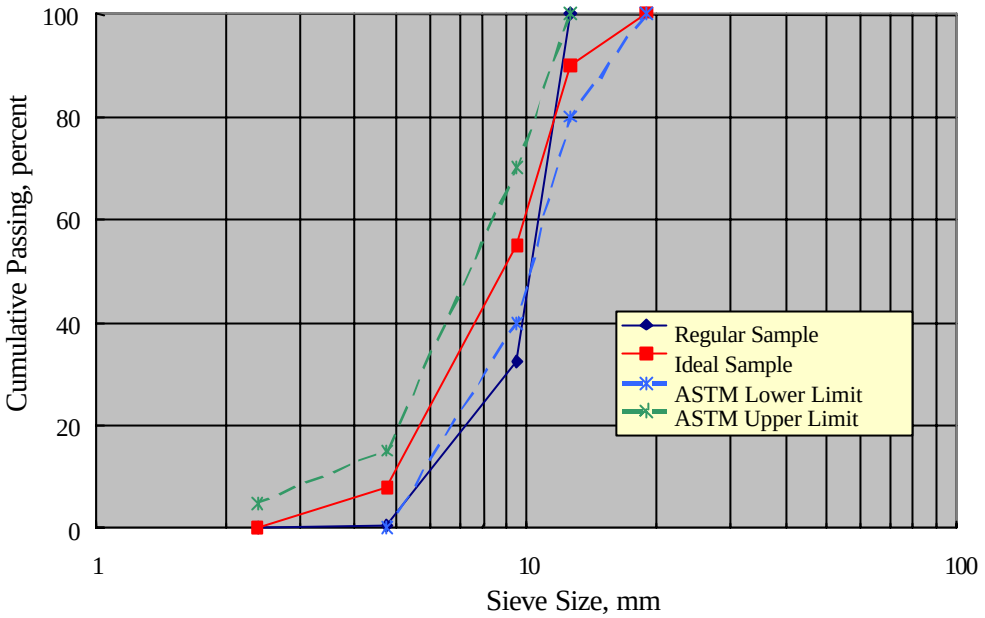

Figure 10: Grading curve for the regular and ideal SLF CA in comparison to the ASTM limits for size number 7.

following steps (14):

1. Upon mining and crushing, the stone is separated into nine stockpiles according to size.
2. The stone from these piles is then batched (blended) according to the specific job specification.
3. The resultant CA is then loaded into a rail car and transported to a concrete plant (trucking may be employed if the distance is short).
4. Upon arrival at the concrete plant, the aggregate is bottom dumped from the rail cars into a silo or stored in bins). This can result in an inverted cone with finer particles at the center and coarser at the outside.
5. The aggregate is transported upon a conveyer belt to the mixer. Both FDOT and plant inspectors check the gradation monthly by taking three samplings from the belt, mixing these, and sieving.

The potential short-coming of this method is that the aggregate is segregated on the belt but may be re-proportioned to within an acceptable range when the three segregated samples are mixed. Consequently, the quality control procedure may be flawed. The fact that results of the sieve analysis for the as-received high FM silica sand and CA acquired for the present research were beyond the lower specification limit is consistent with this.

Coarse Aggregate Pore Size Analyses

Concrete permeability, as determined by properties of the cement, FA, and CA components and the interfacial zone between these, is a fundamental property upon which durability depends. In the most general sense, the term permeability expresses the relative ease with which a particular species migrates through the medium of interest in response to a gradient in chemical potential (most often reflected as a pressure or composition differential). In the latter case (concentration gradient), the process is termed diffusion; and Equation 9 applies subject to the transport being Fickian; that is, no sources or sinks for the diffusing species are present within the medium volume of interest. Porosity, on the other hand, is the void-to-total volume ratio, normally expressed as a percentage. Porosity and permeability may or may not be interrelated depending upon the extent of pore interconnectivity. Thus, permeability of a material with a high density of poorly interconnected pores may be low, while this parameter can be high in the case of well interconnected pores, even when density for the latter is low.

The problem of characterizing transport through porous materials such as concrete is complicated by the fact that there are multiple test methods and intrusion mechanisms; for example, capillary suction, diffusion, and electro-osmosis, each of which can be sensitive to exposure conditions. In general, the available tests methods provide a parameter that is in some manner related to permeability, porosity, or to a combination of the two. The situation is complicated further with attempts to relate a measured parameter that reflects permeability to a form of durability such as freeze-thaw resistance or, in the present case, Cl^- intrusion rate.

Intrusion mercury porosimetry (IMP) and the Iowa Pore Index (IPI) test have been extensively employed for characterization of coarse aggregates. The former involves recording the quantity of mercury that becomes injected into an aggregate sample as pressure is incrementally increased. Because mercury does not wet most materials, including aggregates, the record reflects progressive uptake by decreasing size pores; and from this, plots of cumulative uptake versus pore diameter and pore surface area are generated. Thus, the pore size/area distribution is determined. The IPI, on the other hand, pressurizes a sample using potable water at 0.24 MPa (35 psi); and the water uptake after one and 14 minutes is recorded. The first of these parameters (water uptake after one minute) is indicative of water being absorbed into relatively large pores and, hence, of the volume fraction and interconnectivity of such pores. The higher this water absorption (number), the easier it is for water to drain from the capillary pores,

which is important in the case of freeze-thaw resistance. The second number (14 minute water uptake) indicates the quantity of water that enters the capillary pores. Durability has been reported to be relatively low when the second number exceeds 25. However, the Iowa definition of "durability" presumably pertains to or at least incorporates freeze-thaw resistance, which, of course, is of little relevance in Florida. Thus, while good freeze-thaw resistance should be associated with a high first number and low second, it can be reasoned that good resistance to diffusion of a contaminating species such as chlorides should be realized when both numbers are low.

Mercury Porosimetry and Iowa Pore Index Test Results

As a part of this research, the three CA types were characterized using both IMP and IPI tests. Figures 11 and 12 show the IMP results as plots of cumulative pore area and volume versus pore diameter, respectively, and indicate that the cumulative pore surface area and volume profiles track each other only in a general sense. Steepness of a particular curve is indicative of either the pore volume or surface area change within the applicable size range. Comparisons and conclusions must take into account the logarithmic coordinates. With this in mind, the traces for the SLF and VLA materials are generally similar, albeit with the cumulative volume and area for the former exceeding that of the latter by about a factor of two. Pore volume for the QO aggregate is less than for the SLF and VLA over the entire size range. The relative steepness of the QO surface area-diameter record compared to the volume-diameter one is indicative of the smallest pores in this material having a comparatively high surface area. This resulted in the cumulative surface area of the QO and SLA aggregates being essentially the same, although the pore volumes of the latter exceeded that of the former by a factor of about four.

A previous study (15) reported IMP determinations performed upon CA samples from six quarries that are utilized in conjunction with Florida concrete bridge construction. Figure 13 presents the results from these determinations in comparison to the three CAs that were employed in the present study. This indicates that the three present materials fall within the band represented by the previous six. Of these, the Calera sample, which is a dense Alabama limestone and, as such, should be comparable to the VLA, exhibited the least porosity, followed by the QO material. The SLF, on the other hand, is of comparatively high pore volume.

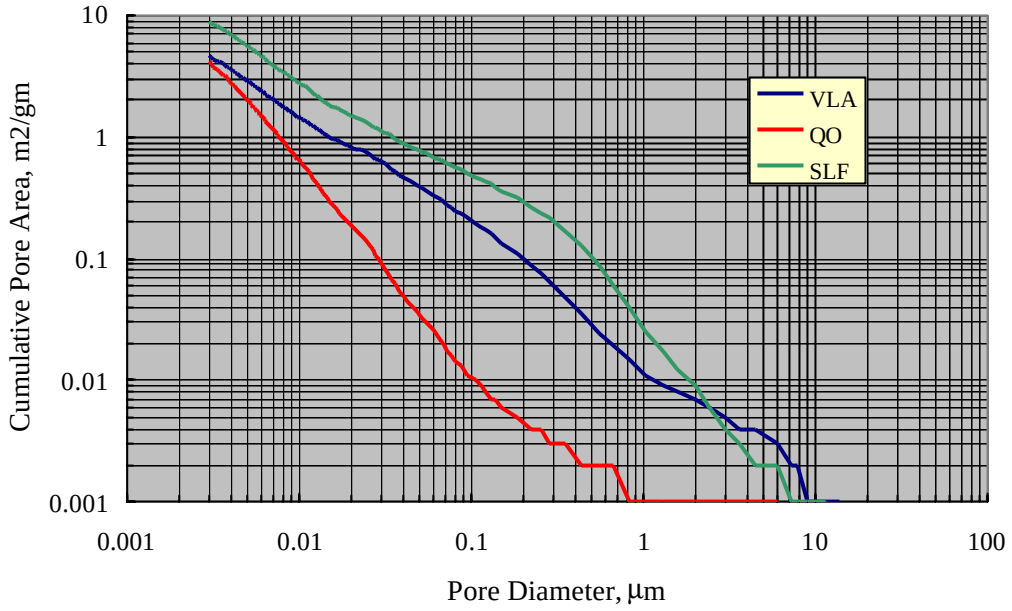

Figure 11: Plot of cumulative pore surface area versus pore size for samples of each of the three coarse aggregates.

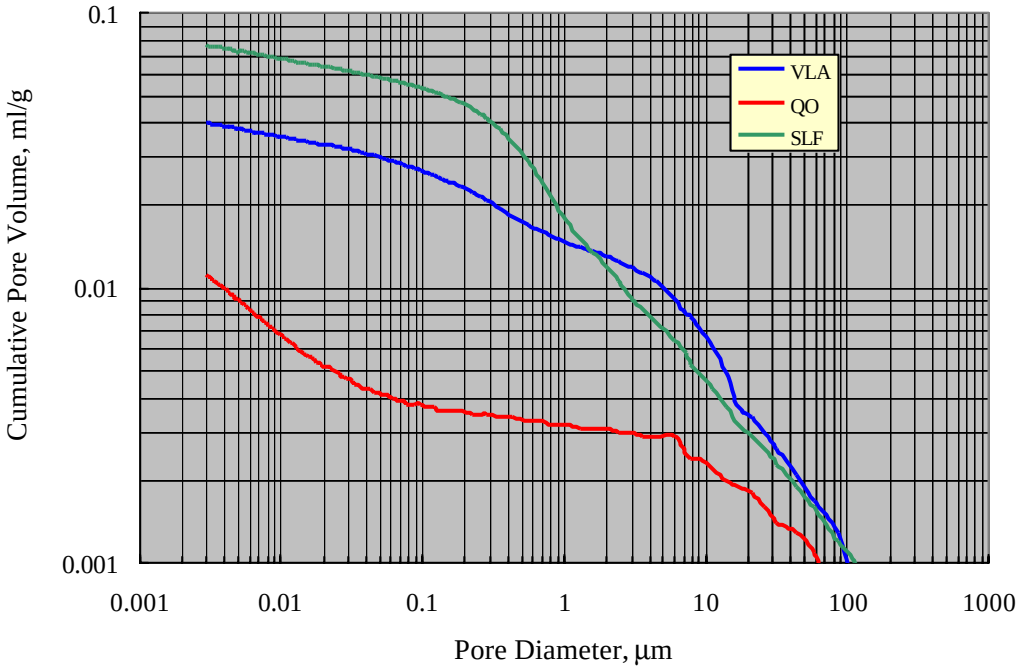

Figure 12: Plot of cumulative pore volume versus pore size for samples of each of the three coarse aggregates.

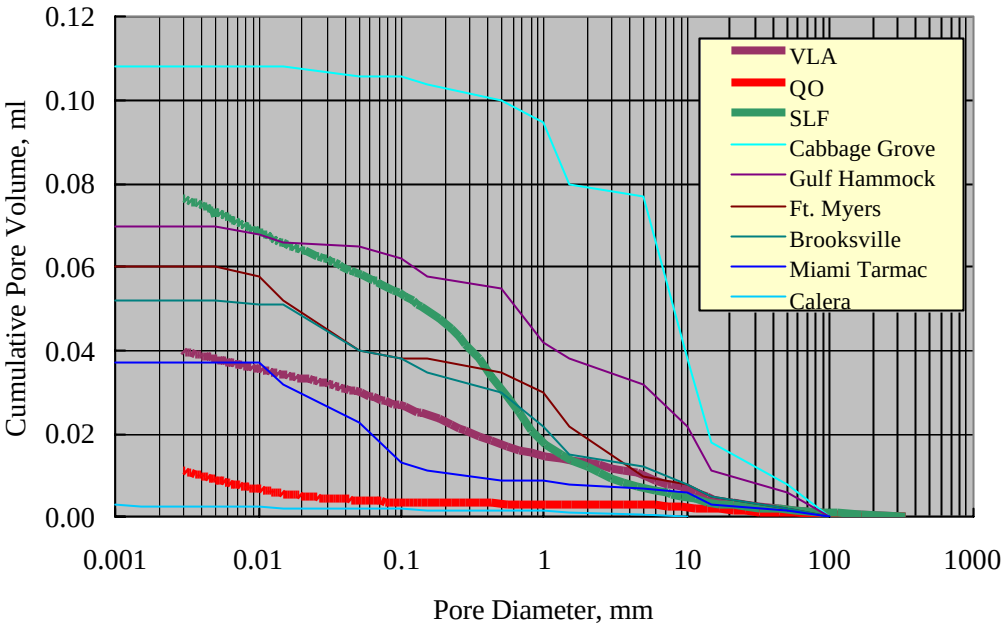

Figure 13: Plot of cumulative pore volume versus pore size for coarse aggregate samples from the previous study (13) in comparison to the present.

Results from the IPI test (Table 9) indicate that relatively large quantities of water were absorbed by the SLF aggregate at both measurement increments (one and 14 minutes) compared to the other two materials, presumably indicating a high pore density/interconnectivity of both large and capillary pores for the SLF. While this difference is consistent with the IMP results for the QO aggregate, it is not for the VLA whose record generally tracked that of the SLF. This may reflect the fact that the two tests are based upon different methods and parameters such that an expectation of a one-to-one comparison is unrealistic. Also at issue is that IMP utilizes a single CA particle, whereas the IPI employs a nine kg sample such that statistical variations are more likely to be an issue for the former than the latter. Clearly, however, both tests indicate that the SLF aggregate has a more developed pore structure compared to the other two materials.

Table 9: Results of the Iowa Pore Index tests.

Aggregate Type	Aggregate Designation	Iowa Pore Index
Southdown Fla. Limestone	SLF	208/44
Vulcan Alabama Limestone	VLA	0/2
Sidley Ohio Quartz	QO	12/2

Chloride Analyses

Procedure Qualification. The FDOT Cl^- analysis method (13) has been established for several decades such that sufficient experience has been gained to qualify it as acceptably accurate. With this in mind, emphasis was placed here upon sample consistency and representativeness. In this regard, Figure 14 shows [Cl^-] as a function of depth for duplicate analyses performed upon samples of the same powder that was obtained from individual mortar slices of Specimen L45-2. Here, the average normalized difference between the duplicate samples was 5.4 percent. Similarly, Figure 15 shows analysis results for specimen L55-1, where data for samples 1 and 2 are for two samples of the same powder (same procedure as for specimen L45-2 (Figure 14)) and those for sample 3 are for powder from a different portion of the same mortar slice. In the former case (L55-1(1) and L55-1(2)), the average normalized difference is 7.4 percent (in making both this and the L45-2 calculation only samples to a depth of 38 mm were considered). For samples L55-1(2) and L55-1(3), on the other hand, the normalized difference is 28.6 percent. In the case of duplicate analyses, the difference in results should reflect accuracy of the procedure alone, whereas for the multiple analyses the difference reflects both this and the heterogeneous nature of the mortar. Table 10 lists the data in Figures 14 and 15 in tabular form.

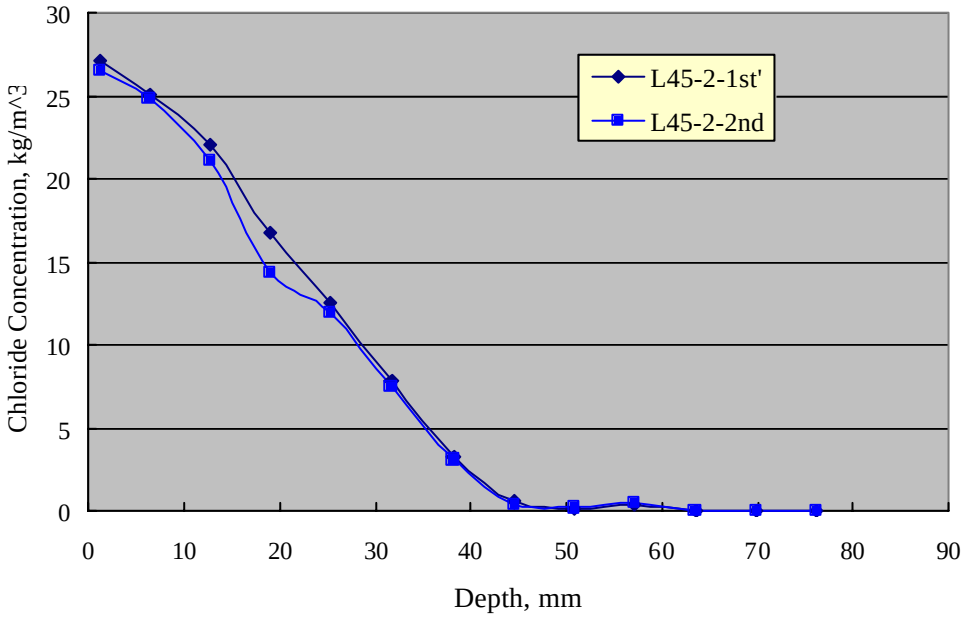

Figure 14: Results of Cl^- analyses performed upon two samples of the same mortar powder acquired from Specimen L45-2.

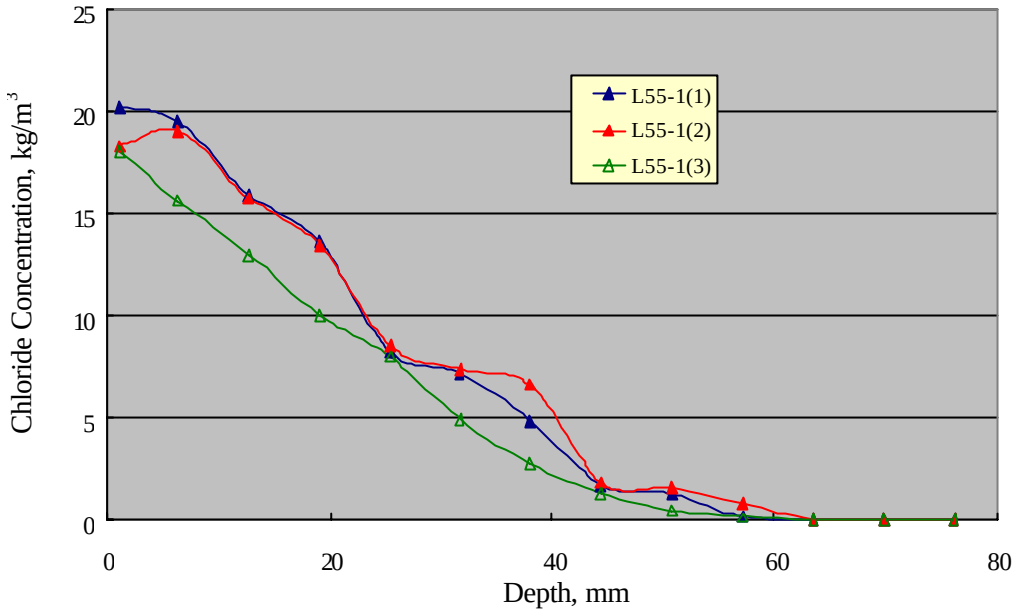

Figure 15: Chloride analysis results for duplicate (same powder) and multiple (different parts of same slice) samples as a function of depth for mortar specimen L55-1.

Table 10: Chloride concentration data (kg/m^3) for duplicate and multiple Cl^- analyses performed upon samples from Specimens L45-2 and L55-1*.

Depth, mm	L45-2(1)	L45-2(2)	L55-1(1)	L55-1(2)	L55-1(3)
1.1	27.070	26.570	20.210	18.290	18.040
6.4	25.170	24.850	19.520	19.090	15.610
12.7	22.100	21.110	15.930	15.760	13.010
19.1	16.720	14.350	13.630	13.480	10.050
25.4	12.530	11.980	8.230	8.540	7.990
31.8	7.870	7.500	7.190	7.380	4.910
38.1	3.260	3.080	4.810	6.600	2.710
44.5	0.530	0.350	1.720	1.830	1.310
50.8	0.060	0.150	1.300	1.570	0.480
57.2	0.330	0.510	0.160	0.830	0.120

* Nomenclature: L – Low FM silica sand.
First two digits – w/c (percent).
Third digit – sand/cement ratio.

Analysis results of slices from 1) the central 51 mm diameter core and 2) the remaining outer ring of specimen L55-2 are listed in Table 11 and shown graphically in Figure 16. These indicate that [Cl^-] was consistently higher near the periphery compared to the central region;

however, the difference was not considered significant. Based upon this, all other sampling and analyses of mortar specimens utilized slices of the full cross section.

Table 11: Chloride analysis results for the central and exterior portion of sections acquired from Specimen L55-2.

Depth, mm	Chloride Conc., kg/m^3		Difference, percent
	Inside	Outside	
3.2	20.82	22.08	5.9
15.9	16.29	18.28	11.5
22.2	13.05	14.68	11.8
34.9	6.44	7.56	16.0
54.0	3.73	3.78	1.3

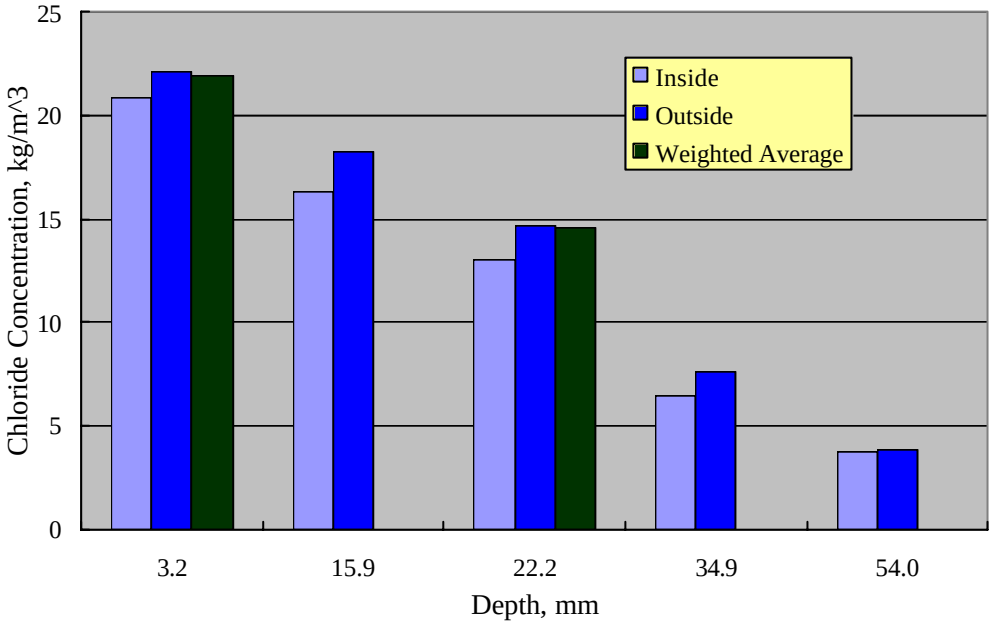

Figure 16 Comparison of [Cl^-] for the center (inside) and periphery (outside) of specimen L55-2 as a function of depth.

Low Fineness Modulus Silica Sand Mortar Specimens. Table 12 lists [Cl^-] for the low FM mortar specimens (other than those listed in Table 10) at the depths for which analyses were performed. Several trends are apparent, each of which is identified below. Thus, Figure 17 plots [Cl^-] versus depth for w/c = 0.55 specimens of the four investigated sand-cement ratios (0, one-half (H), 1, and 2). Of these profiles, the Cl^- penetration for L55-0 and L55-2 exceeded those for L55-H and

L55-1 by a depth average of 13 percent. Considering the variation that was apparent in Figure 15, however, this difference may not be statistically significant.

Interestingly, the four profile slopes in Figure 17 are approximately the same, meaning that the D_{eff} values should also be similar. Table 13 lists D_{eff} for each of these four mix designs and

Table 12: Chloride concentration data (kg/m^3) of samples acquired at different depths from mortar specimens with low FM silica sand.

Depth, mm	L38-H	L38-1	L45-H	L45-1	L55-0	L55-H	L55-2
1.1	22.910	18.860	17.800	20.950	21.210	19.760	22.460
6.4	15.120	12.980	13.660	13.930	20.780	16.630	21.590
12.7	10.470	9.070	11.270	10.420	17.630	14.240	18.150
19.1	4.230	3.410	6.020	5.850	14.030	9.550	14.960
25.4	0.430	0.280	2.570	2.560	11.110	7.750	11.370
31.8	0.050	0.040	0.520	0.620	8.170	3.930	7.570
38.1	0.000	0.010	0.000	0.060	3.290	1.810	3.800
44.5	0.090	0.000	0.050	0.120	1.820	0.480	1.420
50.8	-	0.000	0.040	0.110	0.290	0.040	0.340
57.2	-	0.000	0.030	0.040	0.260	0.040	0.170

Nomenclature: L – Low FM silica sand.
First two digits – w/c (percent).
Third digit – sand/cement ratio.

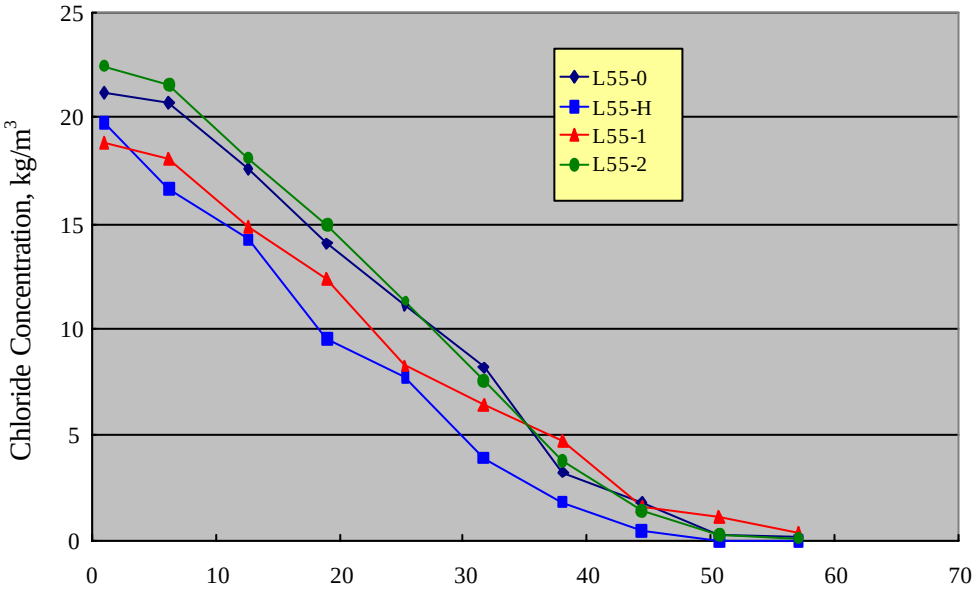

Figure 17: Chloride profiles versus depth for low FM mortar specimens with w/c = 0.55 and sand-cement ratios of 0, 0.5 (H), 1, and 2.

confirms that this was generally the case. Thus, the difference in Cl^- penetration for the L55-0 and L55-2 specimens compared to L55-H and L55-1, assuming this to be real, does not reflect differences in diffusability per se but, instead, in c_s, the surface concentration for this species (see Equation 9). Figure 18 illustrates this graphically as a plot of both D_{eff} and c_s versus w/c. This shows minimal difference in the D_{eff} values at w/c = 0.38 and 0.45, in contrast with the generally recognized trend where these two parameters increase in proportion to one another. This is thought to have resulted from the fact that a superplasticizer was not employed such that the 0.38 w/c mix had virtually no slump and was difficult to place. On the other hand, D_{eff} at 0.55 w/c was

Table 13: Effective Cl^- diffusion coefficients for low FM mortar specimens with w/c = 0.55 and sand-cement ratios of 0, 0.5 (H), 1, and 2.

	Effective Diffusion Coefficient, m^2/s (in^2/y)
L55-0	1.19E-11(0.58)
L55-H	7.90E-12 (0.39)
L55-1	9.05E-12 (0.44)
L55-2	9.56E-12 (0.47)

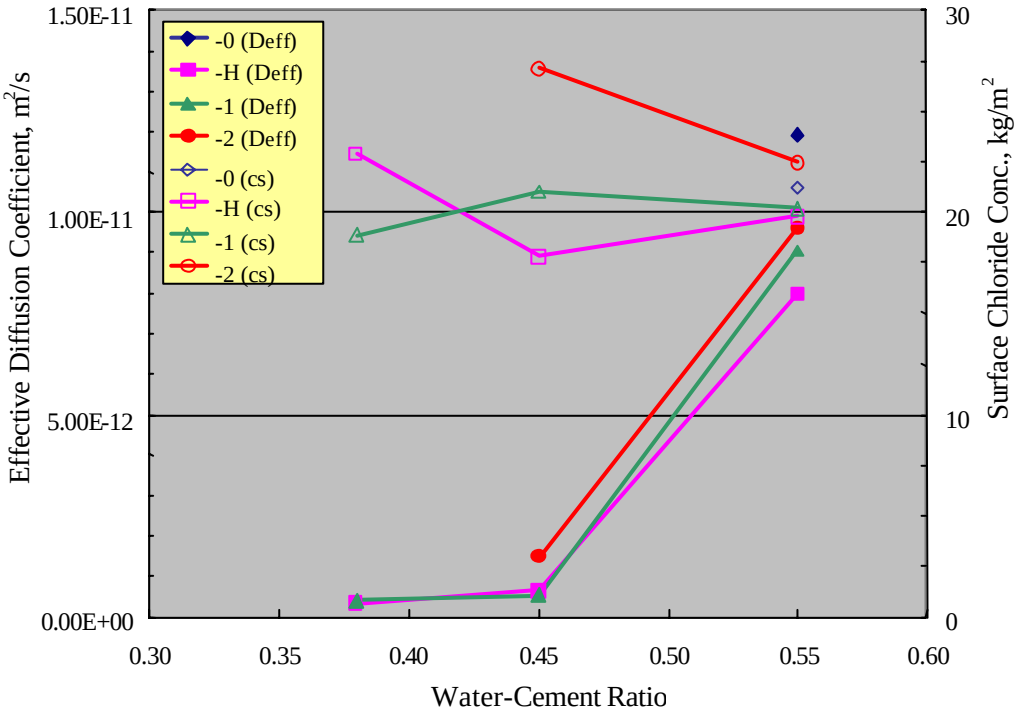

Figure 18: Plot of D_{eff} and c_s for the different low FM mortar specimens.

almost one order of magnitude greater than for 0.45. There is no clear indication that c_s was significantly affected by w/c.

High Fineness Modulus Silica Sand FA Mortar Specimens. Table 14 lists [Cl^-] for the mortar specimens with high FM silica sand fine aggregate at the depths for which samples were acquired. Of these, Figure 19 plots [Cl^-] versus depth for w/c = 0.38 specimens of the three investigated sand-cement ratios (one-half (H), 1, and 2). Correspondingly, Table 15 lists the D_{eff} value for these three profiles and indicates that this parameter was lowest for the H38-1 mix specimen. Figure 20 plots D_{eff} and c_s versus w/c for all specimens that were analyzed. Here, the D_{eff} data for the 0.38 w/c specimens are subject to the same concern expressed above for the low FM ones. This aside, the limited results indicate the D_{eff} was minimum for the one-to-one sand-cement mix and was greatest at w/c = 0.55. There are insufficient data to disclose any dependence of c_s upon w/c.

Table 14: Chloride concentration data (kg/m^3) for samples acquired at different depths of low FM silica sand mortar specimens.

Depth, mm	H38-H	H38-1	H38-2	H45-2	H55-2
1.143	13.07	10.36	12.12	16.98	15.72
6.35	7.15	3.06	8.18	8.79	12.90
12.7	2.86	0.31	4.73	5.83	9.05
19.05	0.18	0.09	0.09	1.43	6.30
25.4	0.07	0.08	0.00	0.07	2.74
31.75	0.07	0.08	0.02	0.01	0.63
38.1	0.05	0.04	0.00	0.01	0.41
44.45	0.07	0.06	0.04	0.00	0.31
50.8	-	-	-	-	-
57.15	-	-	-	-	-

Concrete Block Specimens

Effect of Water-Cement Ratio. Table 16 lists [Cl^-] data for all concrete block specimens as a function of depth below the exposed surface. Correspondingly, Figure 21 plots these data for specimens with the SLF CA of regular (as-received) grading and a cement content of 400 kg/m^3, with the representation being in terms of both w/c and FA:CA:cement ratio (see Table 7). The

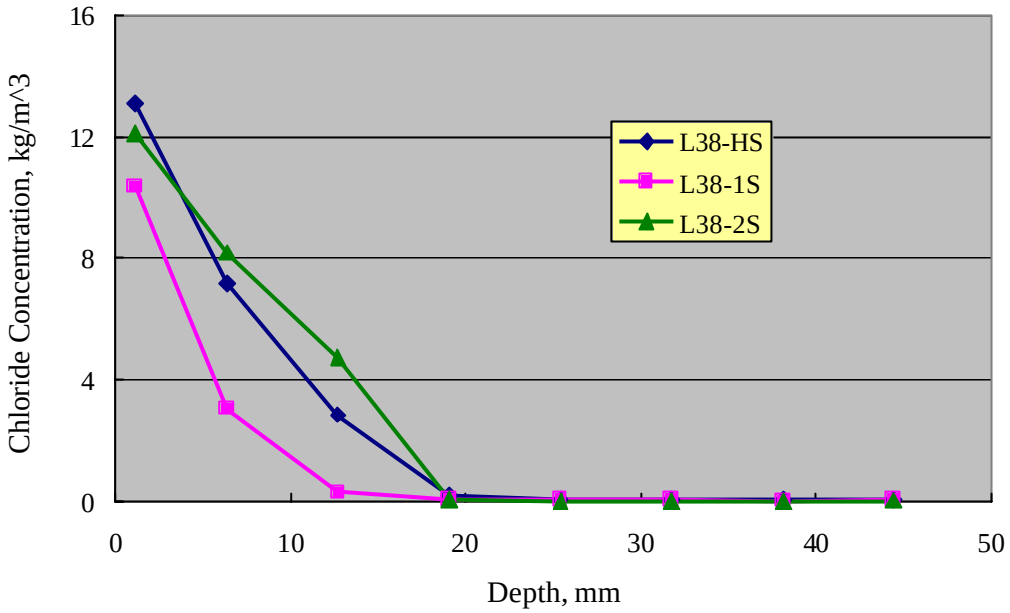

Figure 19: Chloride profiles for silica sand FA mortar specimens with w/c = 0.38 and sand-cement ratios of 0.5 (H), 1, and 2.

Table 15: Effective diffusion coefficient corresponding to the Cl^- profiles in Figure 19 (m^2/s (in^2/y)).

H38-H	H38-1	H38-2
1.11E-12 (0.05)	5.02E-13 (0.02)	2.24E-12 (0.12)

trends indicate that the highest [Cl^-] at a given depth generally corresponded to the lowest w/c. Table 17 lists the D_{eff} values that were calculated based upon the data in Figure 21, and Figure 22 plots these graphically with the data partitioned according to CA-to-FA ratio. As such, specimens with this ratio above 1.19 (SLF3, SLF7, and SLF11) were categorized as "high" (*h*), for a ratio of 1.00 (SLF1 and SLF5) as "medium" (*m*), and for a ratio of 0.70 and below (SLF2 and SLF6) as "low" (*l*). The results are similar to those for the mortar specimens (Figures 20 and 22) in that D_{eff} was lower for w/c = 0.45 than for 0.38, and it is thought that the same explanation (absence of a superplasticizer and poor workability) applies. The fact that c_s for these specimens was relatively high may have resulted from this same cause, although such a trend has been reported by others (9,10). The results for w/c = 0.45, on the other hand, are such that D_{eff} decreased with increasing CA:FA ratio. Figure 23 illustrates this graphically. Because in the present mixes the

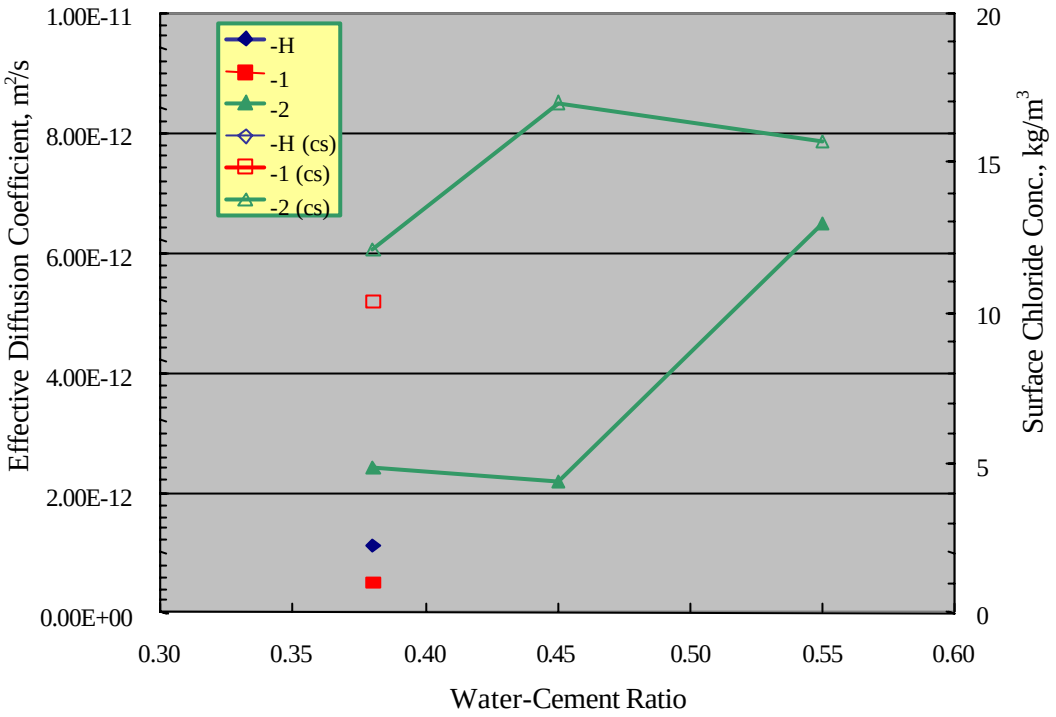

Figure 20: Plot of D_{eff} and c_s as a function of w/c for the different silica sand FA mortar specimens.

CA:FA ratio was directly proportional to the CA volume fraction, the w/c = 0.45 results are consistent with the premise that coarse aggregates provide an impediment to Cl^- ingress.

Figure 24 plots D_{eff} versus w/c for all mortar specimens and specimens with the SLF CA of the regular grading. With the reversal of the normal D_{eff}-w/c trend for concrete specimens with w/c = 0.38 and 0.45 aside, the data generally conform to a common trend of progressively increasing D_{eff} with increasing w/c. The major exception is SLF9 (w/c = 0.45 and D_{eff} = 1.81E-11) which had a relatively low cement content (300 kg/m^3). Also at issue is one or more of the seven low FM mortar specimens with w/c of either 0.45 or 0.55. For these cases where D_{eff} was relatively high, the sand-cement ratio was either zero (paste specimen) or two.

Effect of Cement Content. Figure 25 shows Cl^- profiles for specimens SLF9, SLF1, and SLF10 for which the cement contents were 300, 400, and 500 kg/m^3, respectively (w/c ratio was constant at 0.45). These data indicate that the mix with the lowest cement content clearly exhibited the highest [Cl^-] at a given depth. This was followed by the 500 kg/m^3 cement mix, with the 400 kg/m^3 one having the lowest Cl^- penetration. Table 18 lists the D_{eff} values that correspond to

Table 16: Listing of [Cl] versus depth data for the concrete block specimens.

Depth, mm	SLF1	SLF2	SLF3	SLF4	SLF5	SLF6	SLF7	SLF8	SLF9	SLF10	SLF11	SLF12	OQ1	VLA1
1.1	5.69	4.69	6.07	5.91	7.55	10.14	10.01	7.93	14.51	8.26	5.17	3.99	5.08	6.11
6.4	2.44	2.76	1.71	2.43	3.49	6.02	6.30	3.96	11.05	4.78	2.79	2.20	1.86	2.06
12.7	1.40	1.39	1.30	1.41	2.62	4.12	3.84	2.11	11.82	3.73	2.20	1.52	1.22	1.41
19.1	0.91	0.73	0.76	0.69	1.03	1.88	2.36	1.65	10.47	2.17	1.70	0.89	0.48	0.76
25.4	0.25	0.26	0.30	0.21	0.27	0.53	0.93	0.30	8.73	1.15	0.77	0.58	0.21	0.09
31.8	0.17	0.10	0.16	0.09	0.09	0.24	0.26	0.09	6.90	0.17	0.36	0.17	0.11	0.10
38.1	0.22	0.12	0.09	0.05	0.11	0.18	0.14	0.01	4.46	0.18	0.14	0.08	0.07	0.05
44.5	0.16	0.11	0.17	0.08	0.03	0.18	0.10	0.05	2.85	0.16	0.06	0.06	0.05	0.02

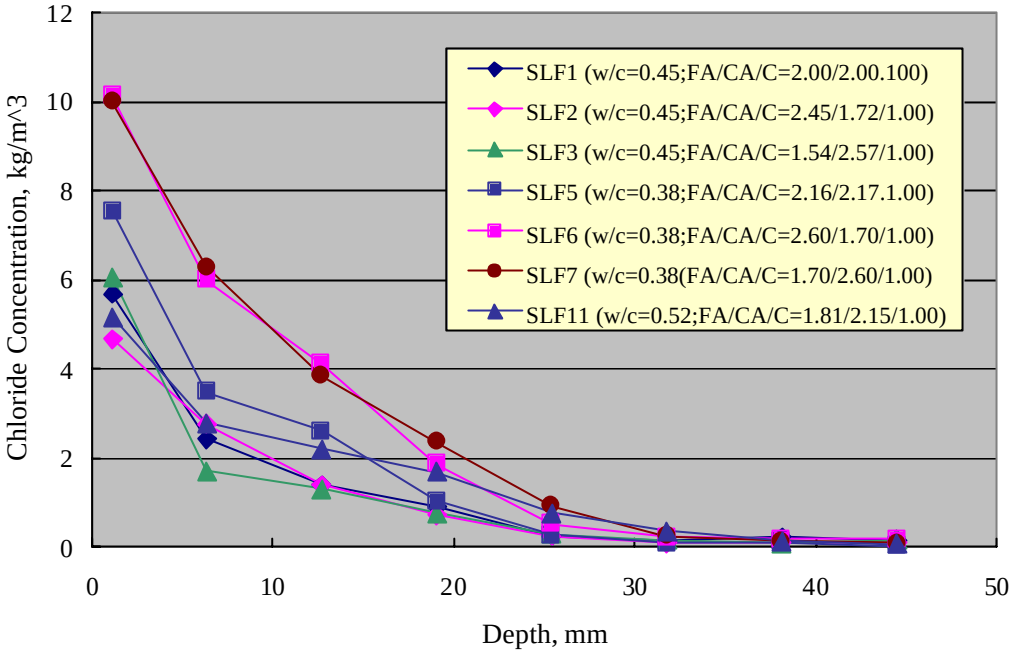

Figure 21: Chloride profiles for "regular" (as-received) SLF coarse aggregate concrete specimens.

Table 17: Effective diffusion coefficient data for the SLF CA mixes with cement content 400 kg/m^3.

w/c	FA/CA/C	Specimen No.	Effective Diffusion Coefficient, m^2/s (in^2/y)
0.38	2.16/2.15/1.00	SLF5	1.78E-12 (0.09)
	2.60/1.70/1.00	SLF6	2.50E-12 (0.12)
	1.70/2.60/1.00	SLF7	2.81E-12 (0.14)
0.45	2.00/2.00/1.00	SLF1	1.31E-12 (0.06)
	2.45/1.72/1.00	SLF2	1.90E-12 (0.09)
	1.54/2.57/1.00	SLF3	5.33E-13 (0.03)
0.52	1.81/2.15/1.00	SLF11	3.95E-12 (0.19)

these data and shows that this parameter was lowest for the 400 kg/m^3 mix (specimen SLF1), although the difference between it and the 500 kg/m^3 specimen (SLF10) may be within the range of expected scatter. Again, the variation in c_s was predominantly responsible for the differences in [Cl$^-$] at a given depth.

Effect of Coarse Aggregate Type. Figure 26 presents [Cl$^-$] profiles for specimens with each of

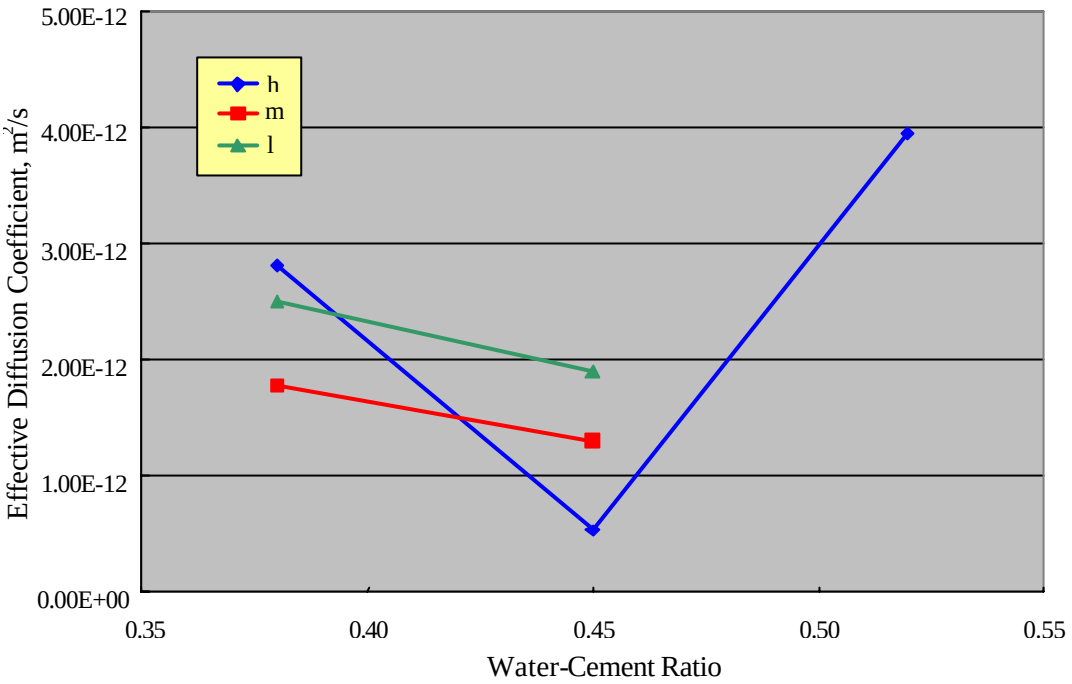

Figure 22: Effective diffusion coefficient as a function of w/c according to high (*h*), medium (*m*), and low (*l*) CA to FA ratios.

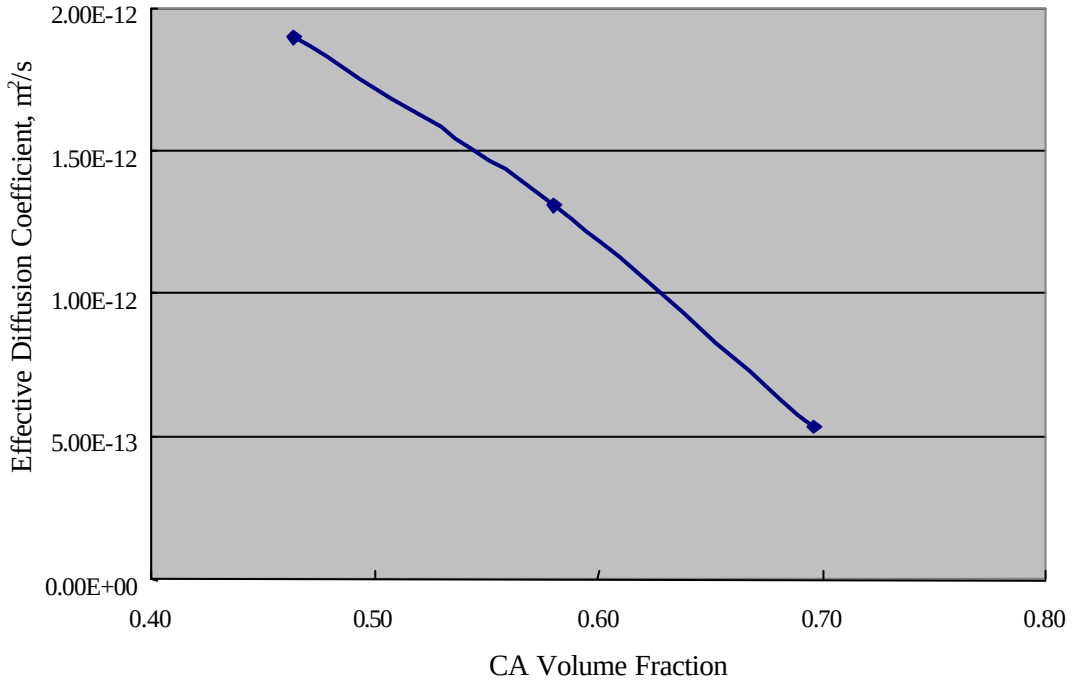

Figure 23: Plot of D_{eff} versus volume fraction CA for concrete specimens with w/c = 0.45.

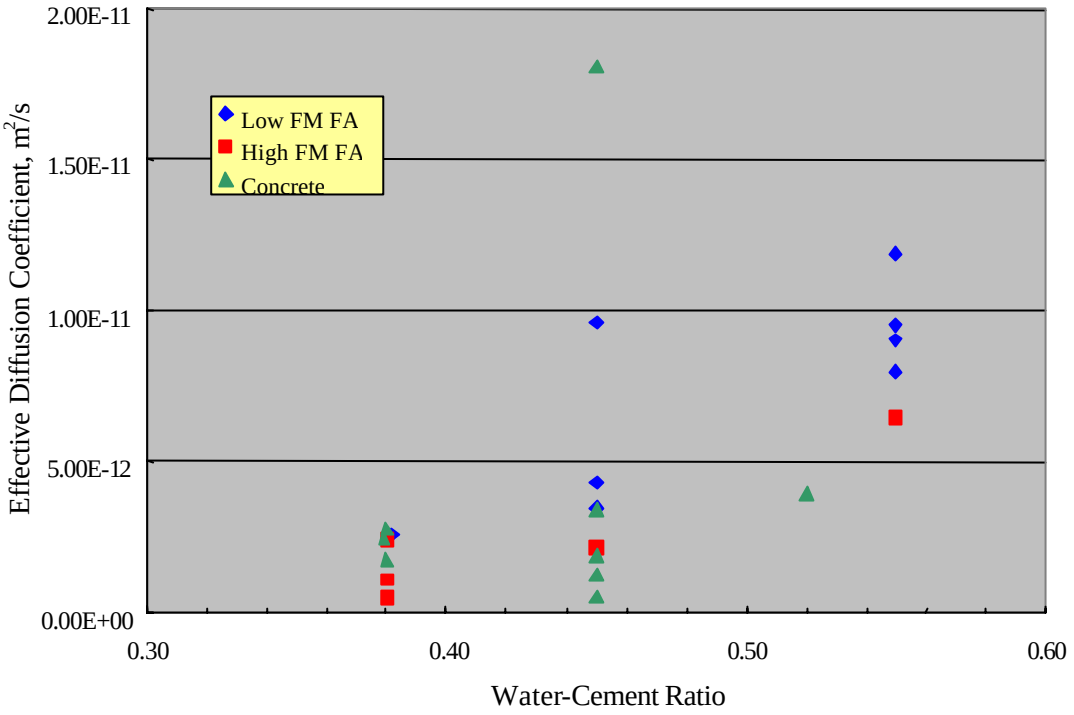

Figure 24: Comparison of D_{eff} values for all mix designs as a function of water-cement ratio.

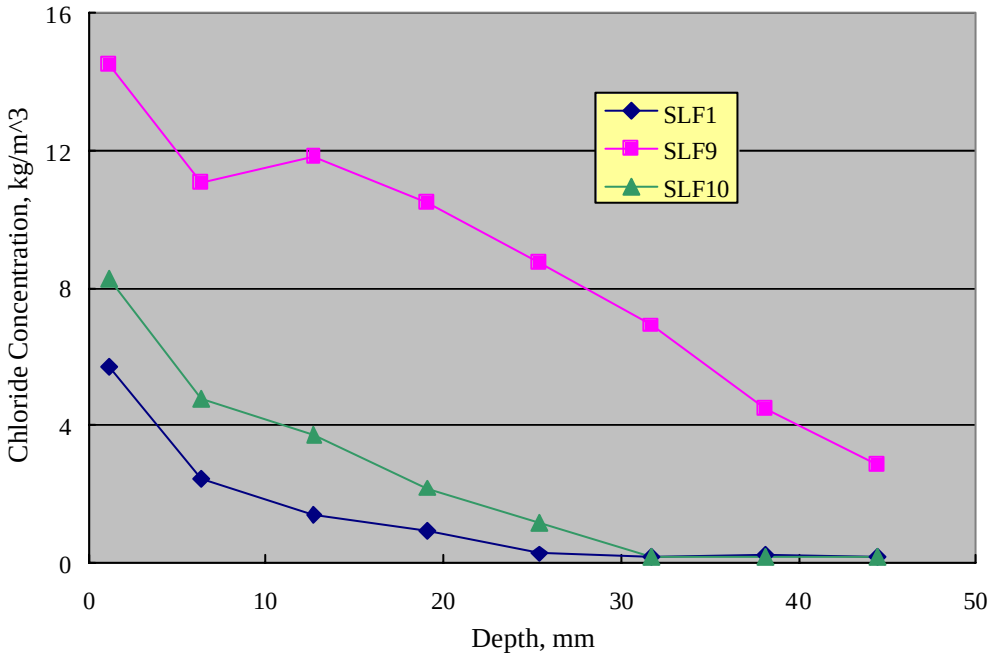

Figure 25: Chloride profiles for specimens SLF1, SLF 9, and SLF 10 with cement contents of 400, 300, and 500 kg/m^3, respectively.

Table 18: Effective diffusion coefficient data for specimens of different cement content.

Specimen No.	S9 (300 kg/m^3)	S1 (400 kg/m^3)	S10 (500 kg/m^3)
D_{eff}	1.81E-11 (0.88)	3.34E-12 (0.06)	4.52E-12 (0.17)

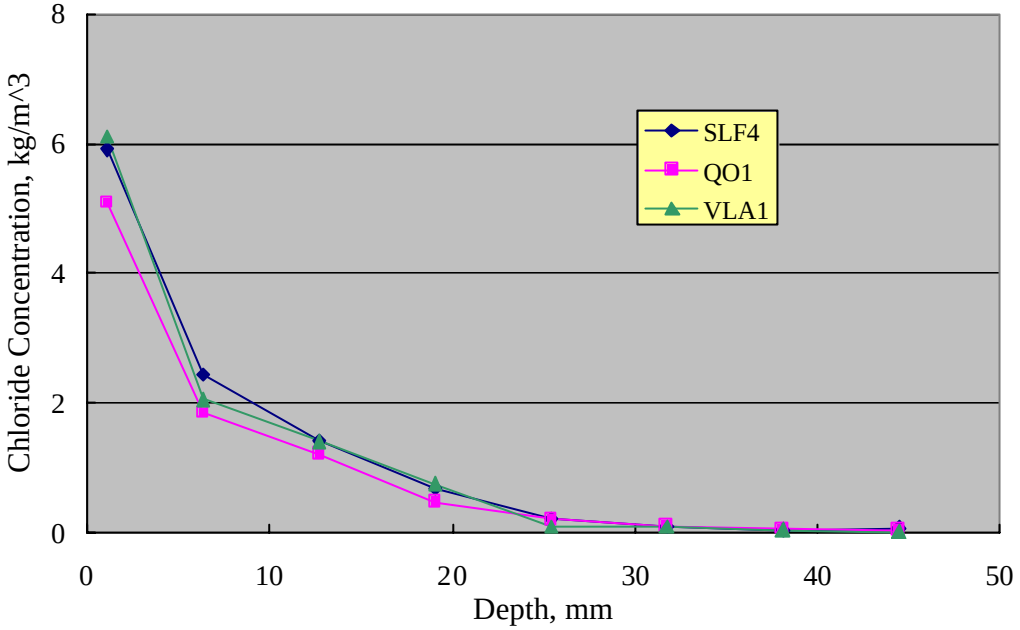

Figure 26: Chloride profiles for concrete specimens with each of the three coarse aggregate types.

the three types of CA, all other mix design factors being the same[1]. With perhaps the exception of a lower c_s for the QO material, the profiles essentially superimpose. Correspondingly, Table 19 lists the D_{eff} values that were calculated for each of these three specimens and shows that this parameter was 16 percent higher than for the SLF compared to VLA CA mix and 26 percent higher than for the QO. Such differences may be within the range of normal scatter. If this is the

Table 19: Effective diffusion coefficient data for specimens with different coarse aggregate types.

Specimen No.	SLF4	QO1	VLA1
D_{eff}	1.11E-12 (0.05)	9.28E-13 (0.05)	8.19E-13 (0.04)

[1] These three mix designs (S4, VLA, and QO) were based upon ideally graded CA rather than regular (as-received).

case, then there is little or no distinction between the D_{eff} values for concrete of the three CA types. This contrasts with the fact that Florida limestones are of relatively high porosity, as confirmed by the data in Figures 11-13 and Table 9, and that the QO material has been projected to be one of the most dense aggregates in the United States (11). At the same time, no studies have been performed where D_{eff} was explicitly determined as a function of CA properties. These findings indicate that material test and characterization methods such as IMP and IPI are of little or no value with regard to qualifying coarse aggregates for Cl^- exposures in which resultant reinforcement corrosion is service life determining. This result is consistent with the projection that chlorides do not reside in or diffuse through Florida limestone CA and perhaps others, and as such, that they provide an impediment to ingress of this species.

A possible explanation for the present finding that the differences in CA porosity did not significantly effect D_{eff} is that pores in the SLF material were dominated by relatively large voids that were not water filled under he low hydraulic head that existed in the present ponding experiments. If this was the case, then moisture and, hence, Cl^- access to capillary pores was accordingly restricted. The finding that the SLF CA exhibited a relatively high IPI Index (Table 9) may have been a consequence of the relatively high pressure that is utilized in this test.

Effect of Coarse Aggregate Gradation. Figure 27 compares the Cl^- profiles for the ideal versus regular graded CA specimens for the three w/c values for which specimens were fabricated (0.38 for specimens SLF5 and SLF8, 0.45 for specimens SLF1 and SLF4, and 0.52 for specimens SLF11 and SLF12, where the first listed specimen of each pair is of the regular grading and the second the ideal). All other mix design parameters were the same in each case. Correspondingly, Table 20 lists the D_{eff} values, and Figure 28 shows these graphically. Focusing upon the 0.45 and 0.52 w/c data in view of the suspect nature of the 0.38 results, as noted above, the ideal graded D_{eff} values are seen to be 16 and 26 percent, respectively, below those of the regular grade. While these differences may be within the range of experimental scatter, still a beneficial effect of the ideal grading compared to the as-received may exist. If the differences are real, then it may be possible, with further mix design modifications or improved quality control (or both), to affect further reductions in D_{eff} based upon grading alone to a point where improvements of practical significance are realized. Even a modest D_{eff} reduction of 16 percent could be significant. For example, Table 21 lists results from calculations based upon Equation 9, where the first row indicates that a concrete cover of 0.073 m (2.89 in), which approximates the current minimum FDOT specification for precast coastal bridge substructure elements, is required for a T_i, of 75

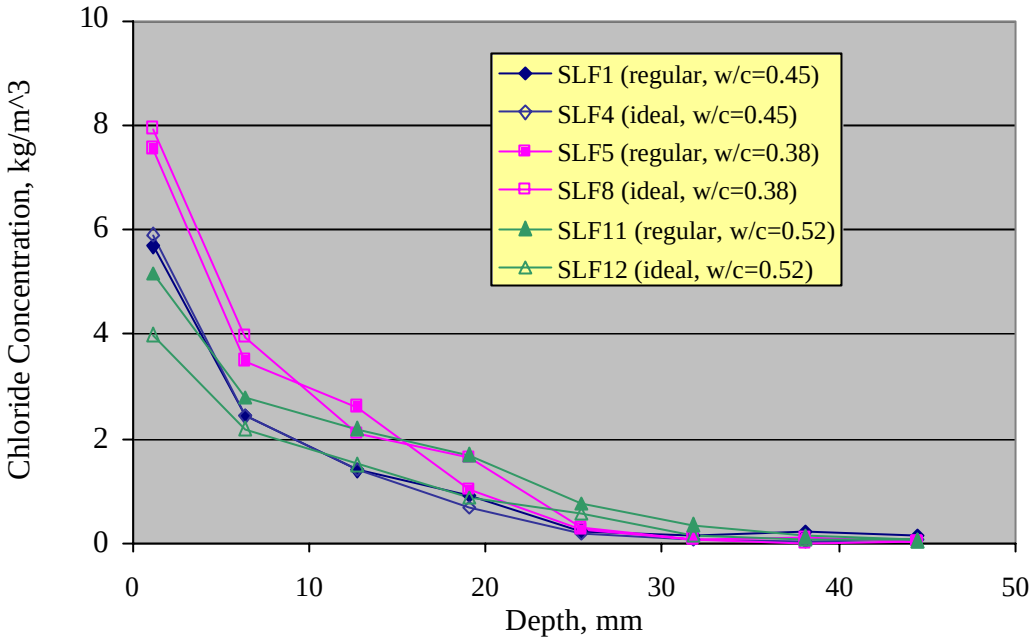

Figure 27: Chloride profiles for comparable concrete specimens with regular versus ideally graded CA and each of the three water-cement ratios.

Table 20: Values for D_{eff} for regular and ideal graded mix designs of three w/c.

Effective Diffusion Coefficient, m^2/s (in^2/y)					
w/c=0.38		w/c=0.45		w/c=0.52	
SLF5 (regular)	SLF8 (ideal)	SLF1 (regular)	SLF4 (ideal)	SLF11 (regular)	SLF12 (ideal)
1.78E-12 (0.09)	1.74E-12 (0.09)	1.31E-12 (0.06)	1.11E-12 (0.05)	3.95E-12 (0.19)	2.91E-12 (0.14)

years assuming c_{th} = 3.54 kg/m^3 (6.0 pcy), c_o = 0, D_{eff} = 1.31E-12 (value for specimen SLF1), and c_s = 10 kg/m^3. However, row two shows that this cover reduces to 0.067 m (2.64 in), a nine percent reduction, if D_{eff} becomes 1.11E-12 (specimen SLF4). Alternatively, for a cover of 0.073 m and the lesser D_{eff}, T_i = 89 years for a 16 percent corrosion-free life enhancement (row three). These improvements are in spite of the fact that the difference between the ideal and regular gradings was relatively modest (Figure 10). A program is recommended to, first, statistically characterize the actual CA and FA gradings that are being realized in Florida bridge concretes and, second, quantify the improvement in D_{eff} that could be realized if these were within specification.

Of possible importance also are distinctions in c_s. While differences in this parameter were

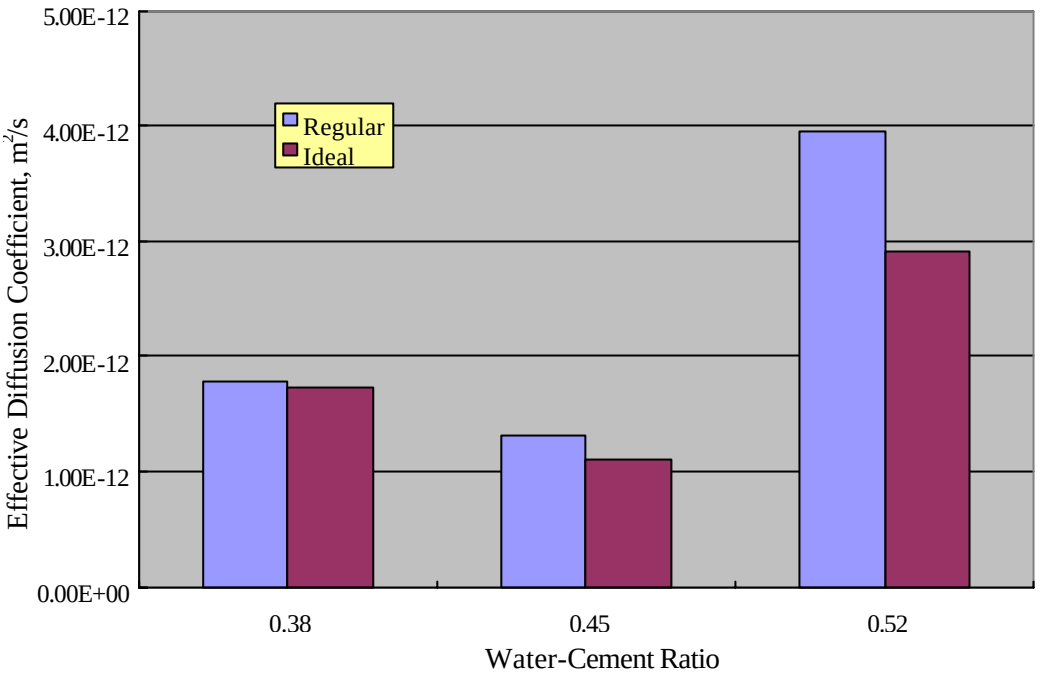

Figure 28: Effective diffusion coefficient data for regular versus ideal graded SLF CA specimens at each of the three w/c values.

Table 21: Comparison of Times-to-Corrosion and required covers based upon D_{eff} results for the ideal and regular graded coarse aggregates.

D_{eff}, m^2/s (in^2/y)	Concrete Cover, m (in)	Time-to-Corrosion, y
1.31E-12 (0.05)	0.073 (2.89)	75
1.11E-12 (0.06)	0.067 (2.64)	75
1.11E-12 (0.05)	0.073 (2.89)	89

essentially nil for the two grading categories at w/c = 0.38 and 0.45, the distinction at w/c 0.52 may be significant. If this is the case, then any added diffusion path tortuosity afforded by the ideal compared to regular grading was important here. However, the w/c for the specimen pair that indicated this is beyond the range of practical importance for modern high performance concretes.

Scanning Electron Microscope (SEM) and Energy Dispersive X-Ray (EDX) Analyses

The fracture surface of some core slices was viewed using a JEOL 6100 SEM, and local sites were analyzed compositionally with a Noran EDX. Only samples from within approximately the top 12 mm were examined because [Cl^-] was relatively high here, and the

sensitivity/accuracy of EDX at concentrations below approximately one percent, as generally existed at greater depths, can be poor.

Figure 29 shows the composition for individual particles of each of the three predominant aggregate types (SLF and high and low FM silica sand). Thus, this CA was comprised predominantly of Ca with minor amounts of Mg, S, and Fe. Both silica sands, on the other hand, were mostly Si but with some Ca. Further analysis indicated that approximately 80 percent of the low FM fine aggregate was silica-rich, presumably as SiO_2, and the remainder Ca-rich ($CaCO_3$). Composition of the silica sand in both FA types (high and low FM) was essentially the same. Figure 30 shows the analysis results for a low FM particle that was Ca rich, presumably a limestone fine. Note, however, that while no Cl^- was detected for the CA or high FM silica sand, including Si-rich FA in the exposed masonry sand specimens, this species was present in the Ca rich FA. This trend, where Cl^- was present in the Ca rich FA particles, may have been responsible for the relatively high c_s of this species exhibited by mortar specimens that utilized this material. Likewise, Figure 31 shows analysis results for the paste area of specimens of both FA types. This indicates Ca, and to a lesser extent Si, were the major components here with minor concentrations of Mg, Al, Fe, and S, as well as Cl^-.

Figure 32(a) is an electron micrograph of a fracture face from specimen SLF7 showing both

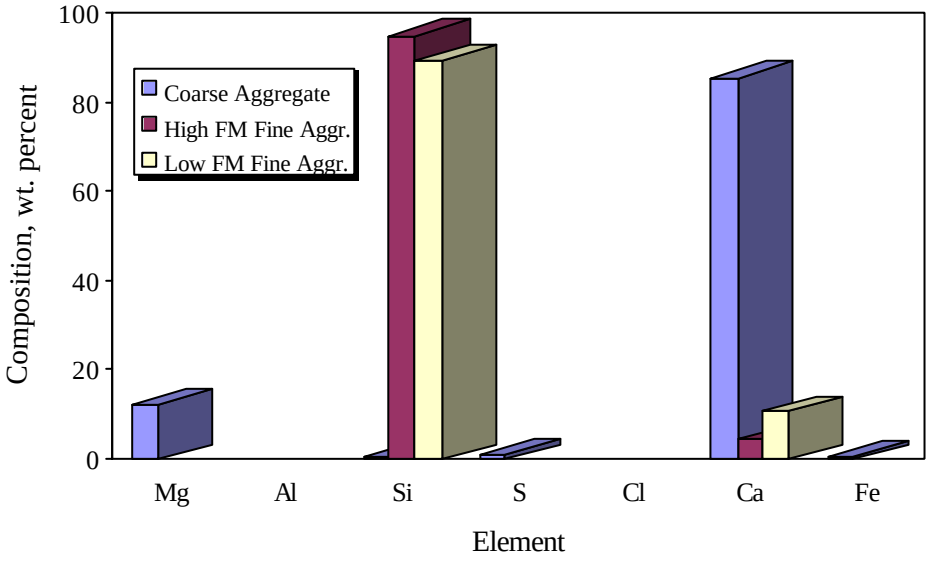

Figure 29: EDX compositional analysis results for samples of the three aggregate types within a mortar/concrete specimen.

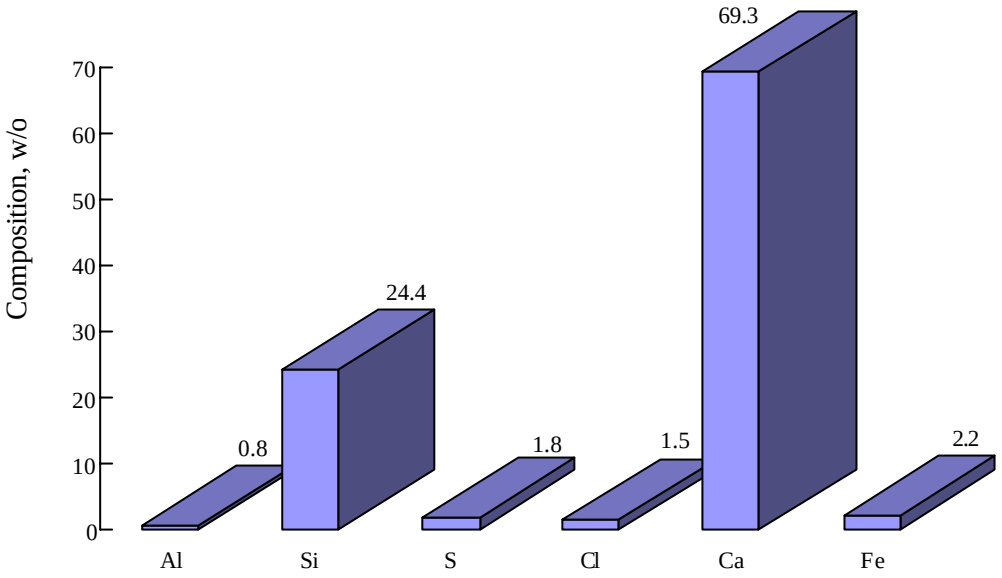

Figure 30: Compositional analysis for a Ca-rich FA particle in a low FM mortar specimen.

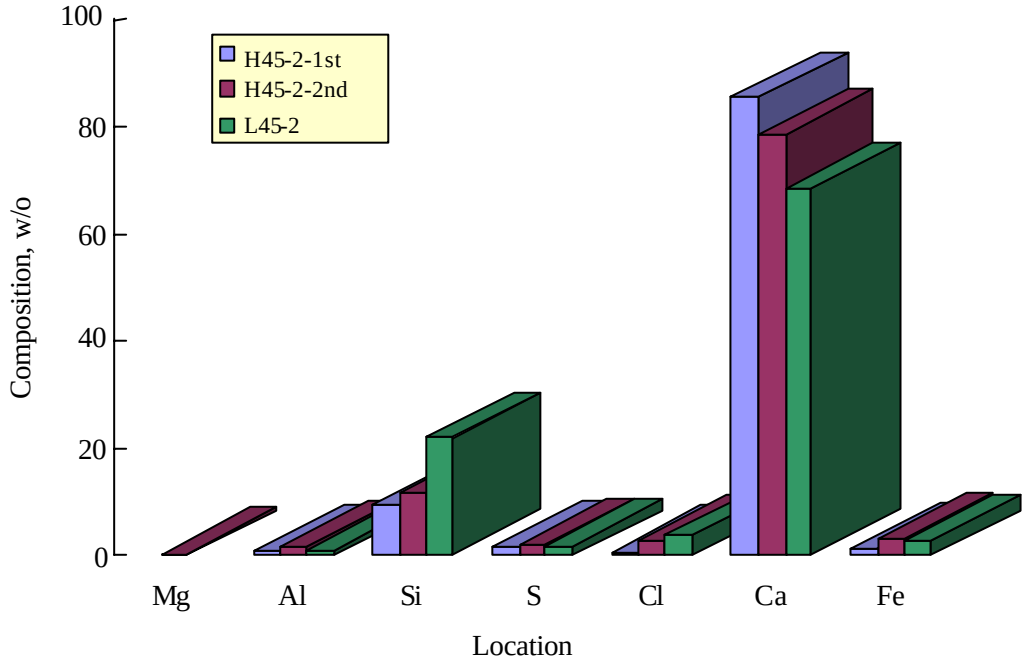

Figure 31: EDX compositional analysis results for cement paste areas of specimens H45-2 (high FM silica sand FA) and L45-2 (low FM silica sand FA).

a coarse and fine (silica sand) particle as well as the cement paste matrix. Also illustrated is the location of seven contiguous EDX spot analyses that traversed the span between the two particles. Figure 32(b) shows the seven Cl^- analysis results and reveals that this species was not detected at

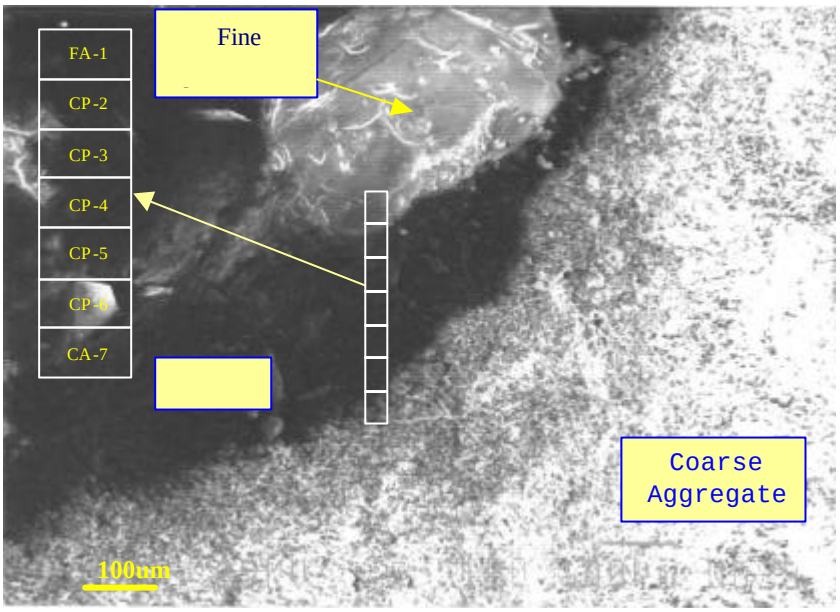

(a)

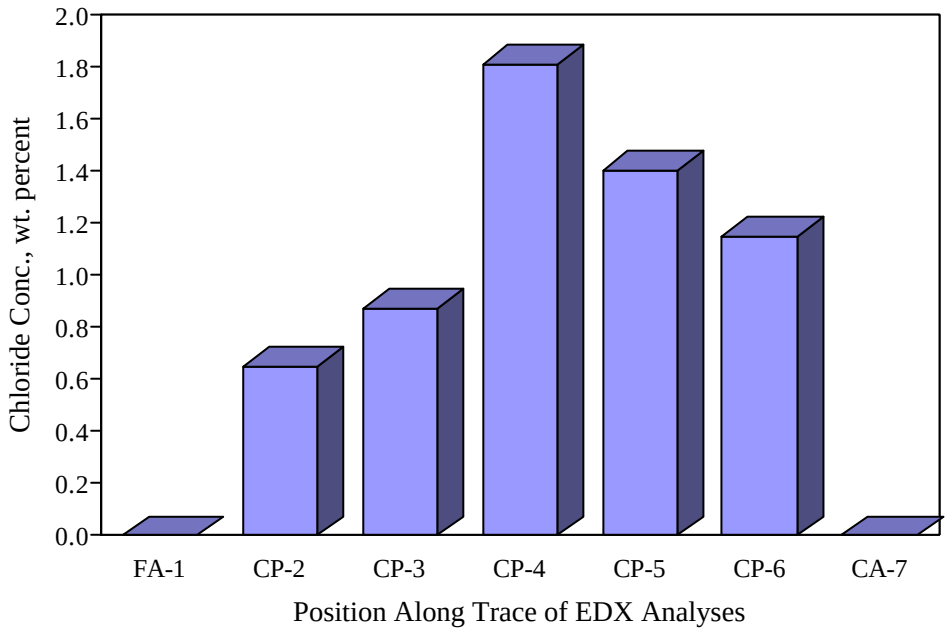

(b)

Figure 32: Scanning electron micrograph (a) of specimen SLF7 showing CA and high FM silica sand particles and cement paste. Locations of EDX scans that traversed the span between the two aggregate particles are also illustrated and (b) Cl^- results.

either aggregate but it was present within the paste. The trend of higher [Cl^-] the greater the distance from either particle may be an artifact whereby some x-rays emitted from the particle(s) were detected even though the analysis area was designated as the paste alone. Alternatively, a diffusional edge effect could have been responsible. These results are in agreement with previous findings, as summarized in Tables 1 and 2 and Figure 5, and with results from the present project that indicated chlorides apparently did not enter the CA or silica sand FA and that these particles served as impediments to inward migration.

It has been projected based upon IMP studies by others that the pore structure of paste is altered when aggregate is introduced such that a transition zone of relatively high porosity and abnormally large pores about 20 μm thick results (17-19). Presence of this zone apparently results in increased permeability of mortar and concrete compared to paste, with the effect becoming disproportionate at an aggregate content in excess of some critical value where the transition zone from neighboring particles begins to overlap (20). Consistent with this, Halamickova et al. (21) reported increased water and Cl^- transport coefficients for mortars compared to paste specimens. Young (22) reported that permeability coefficients for mortars are about 3-10 times greater than for paste and for concretes about 100 times greater. The present results do not agree with these finding since, here, the paste specimen exhibited the largest D_{eff} (specimen SLF9, which had a low cement content (300 kg/m^3), was an exception (see Table 13)). This may have resulted from, first, water permeability rather than Cl^- diffusion being reported in some cases and, second, differences in procedure, where Halamickova et als. experiments were short-term and employed a pressure differential cell in the case of water transmission and an impressed voltage for chlorides. Previous research has shown that poor correlation can result for artificially accelerated versus longer-term, concentration gradient induced Cl^- intrusion (23). On the other hand, the mortar specimens with the highest sand-cement ratio (two) routinely exhibited higher D_{eff} values than for mortar specimens with a lesser sand fraction (Figures 18 and 20). This is consistent with the transition zone occupying an increasing volume fraction of the material as the sand content increased, as proposed by Halamickova et al. (21). Results of the present experiments suggest an effect of two competing processes where transition zone interconnectivity dominated at high sand-cement ratio and aggregate related Cl^- ingress impediment at low. Figure 33 illustrates this schematically. Alternatively, the low FM mortar specimens exhibited interfacial separations to a greater extent than did the high FM silica sand or coarse aggregate particles. This is in spite of the fact that 80 percent of the low FM fine aggregate was silica sand, as noted above. Figure 34 shows a SEM micrograph of a FA particle with separations at the paste

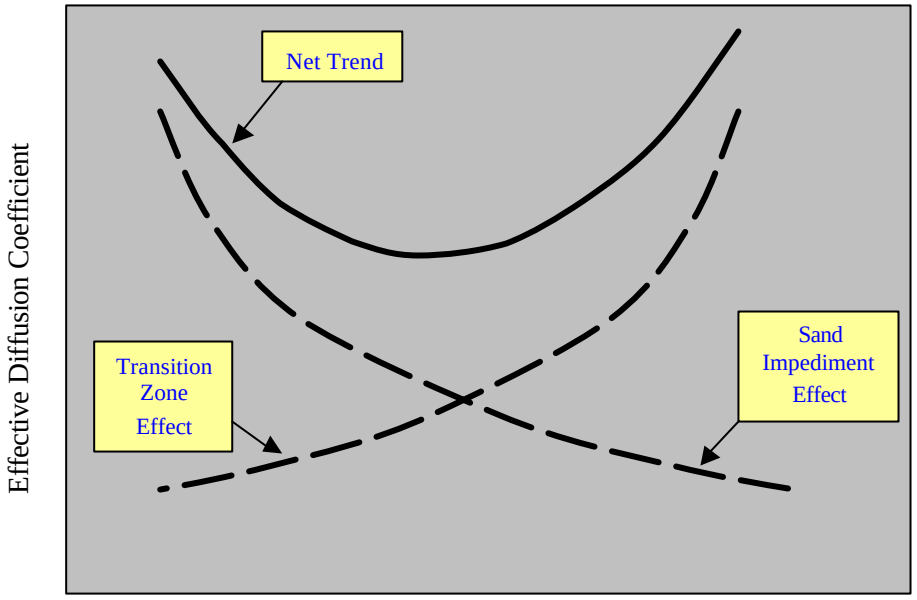

Figure 33: Schematic illustration of the competing affects of sand content in mortar specimens upon D_{eff}.

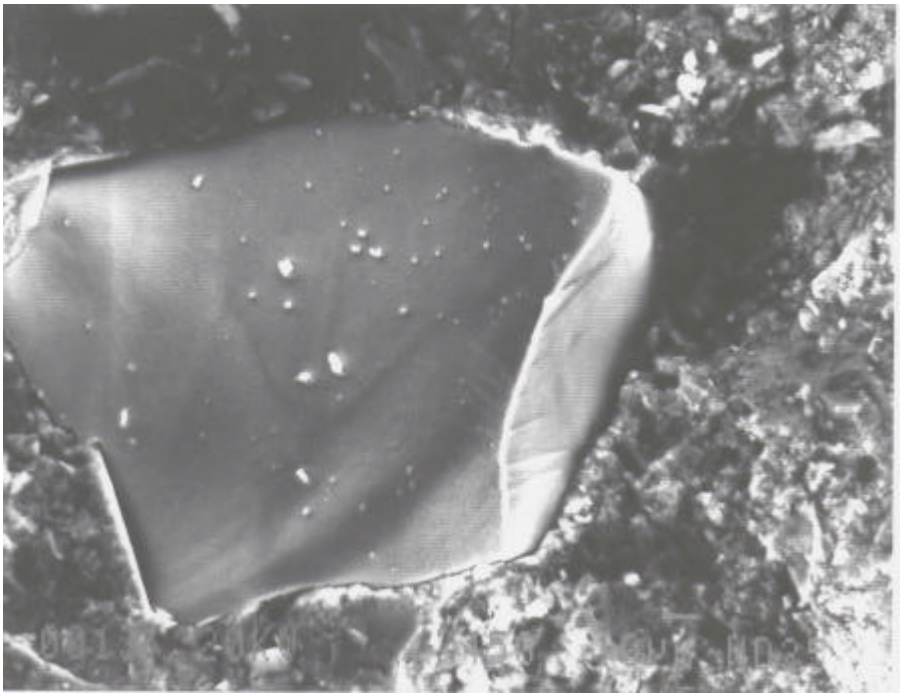

Figure 34: SEM micrograph of a FA particle and cement matrix for specimen L45-2.

interface. The possibility cannot be discounted, however, that the separations as seen here occurred in conjunction with the mortar slice being fractured. Nonetheless, the finding that such separations were more common in the low FM mortar specimens suggests a relatively weak interfacial bond, as could arise from excess porosity.

Another possibility is that no transition zone of high Cl^- permeability existed in the present specimens at the time of analysis. If it were the case, some indication should have been forthcoming from the EDX results in Figure 32, since the analysis spot dimensions approximated thickness of any transition zone. Maso (24) reported that no transition zone was present in well cured systems he investigated.

This observation that D_{eff} for both FA types was minimal at a sand-cement ratio of about unity (one-half in the case of the low FM mortar) and was elevated for a value of two, the effect being greater for high compared to low FM mortar (see Tables 15 and 13, respectively), raises a concern since common concrete mix designs often specify a ratio of about two. If this same effect carries forth to concrete, then the high FM mortar specimen data (Table 15) indicate that a two-fold reduction in D_{eff} would be realized if the sand-cement ratio could be reduced to near one.

The determination that chlorides were present in the Ca-rich low FM fine aggregate but not in the limestone CA could be size related. If this is the case, then it is important that the size transition below which Cl^- uptake occurred for limestone aggregates be determined and that this serve as a lower limit for these CA in the case of concretes that are to be exposed to chlorides in service. No such determination was made as a part of this study, however.

Significance of Surface Chloride Concentration

Virtually all of the Cl^- analysis data and trends related thereto that were developed in the present experiments point to both c_s, and D_{eff}, being important parameters with regard to Cl^- intrusion rate. In this regard, Equation 9 indicates a square root dependence of $[Cl^-]$ upon D_{eff}, whereas the dependence upon c_s is according to a power of unity. Despite this, relatively little attention has been focused in past research upon means whereby c_s might be affected and controlled. An exception is the work of Bamforth and Price (10) and Bamforth (9), who identified 1) location, 2) physical aspects of exposure (for example, orientation, degree of shelter, and micro-climate), 3) mix design variables, 4) curing variables, and 5) type of formwork, as

influential. Bamforth and Price summarized their own results for structures and specimens undergoing coastal exposure in combination with data from the literature and concluded that, first, c_s apparently reached a steady-state value within the initial six months and, second, c_s was variable because of seasonal weather and surface washing. Most of the c_s data for OPC concretes were in the range 0.1-0.8 w/o concrete. Measured values for c_s in the present concrete specimens were 3-10 kg/m^3 of concrete or 0.13-0.45 on a w/o basis, in general agreement with the previously reported range. Bamforth (9) pointed out that c_s increased with increasing cement content, presence of pozollans, and increased curing time. This potentially poses a problem for situations where mix design is durability driven, since D_{eff} exhibits an opposite dependence upon each of these three factors. If this is the case, then optimization of Cl^- ingress resistance may involve a tradeoff with these mix design variables. The latter two factors (pozzolans and curing time) were not included in the present study. This importance of c_s toward understanding the mix design dependence of Cl^- intrusion may be responsible for or have contributed to the relatively poor correlation that has been reported between rapid permeability (charge gradient driven) and natural diffusion (concentration gradient driven) results (20).

Figure 35 shows the present c_s data on a w/o cement basis and indicates that, with three exceptions, values are in the range 1.0-2.7 w/o cement. Also, while the concrete specimen data show decreasing c_s with increasing w/c, no definitive dependence of c_s upon w/c is apparent for mortars of either FA type. This c_s-w/c trend for the concrete specimens is disappointing, although it is consistent with the findings of Bamforth (9), because it indicates a negative consequence of low w/c mix designs for Cl^- exposure service, as noted above. The data suggest that research regarding concrete surface treatments for the purpose of reducing c_s could be advantageous. The exceptions to the general trend whereby c_s was in the range 1.0-2.7 w/o cement are the concrete specimen SLF9, which had the lowest cement content, and specimens L45-2 and L55-2, which had the highest sand-cement ratio (two). Thus, this sand-cement ratio not only elevated D_{eff}, compared to lesser ratios, as noted above, but it also resulted in relatively high values for c_s. In contrast to the above, Figure 36 plots c_s versus D_{eff} revealing a general trend suggesting that material and mix design factors tend to have a common effect upon both parameters, albeit with relatively large scatter. This general trend whereby high c_s tended to result in high D_{eff} may, however, be an artifact of whatever factor(s) caused the outliers (high sand-cement ratio in the case of mortars and low cement content for concrete); and so other aspects of mix design that were not investigated might alter this.

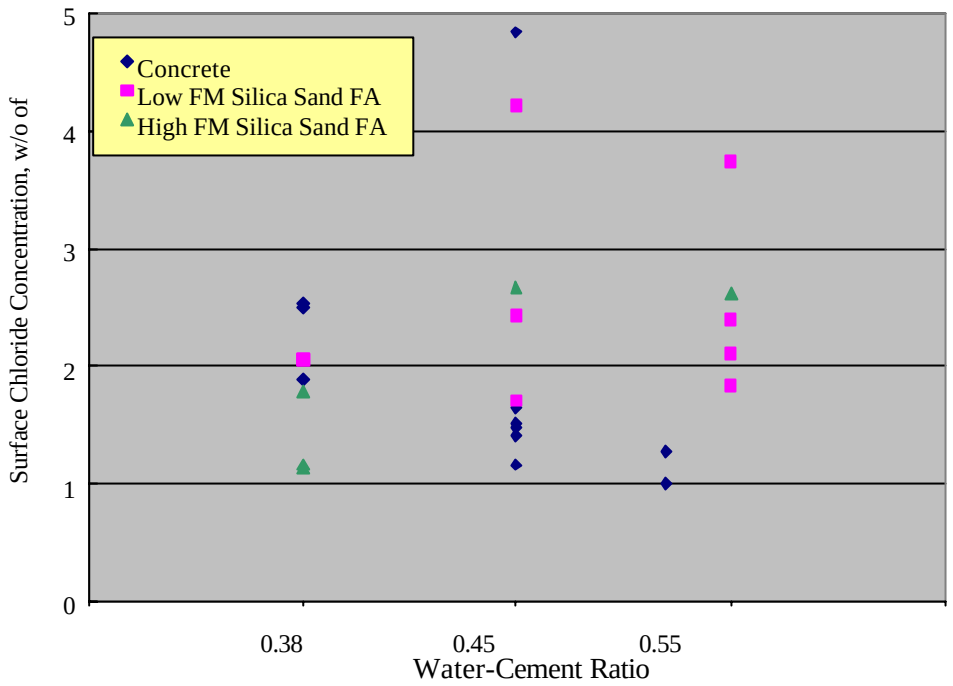

Figure 35: Representation of surface Cl^- concentration on a cement weight basis.

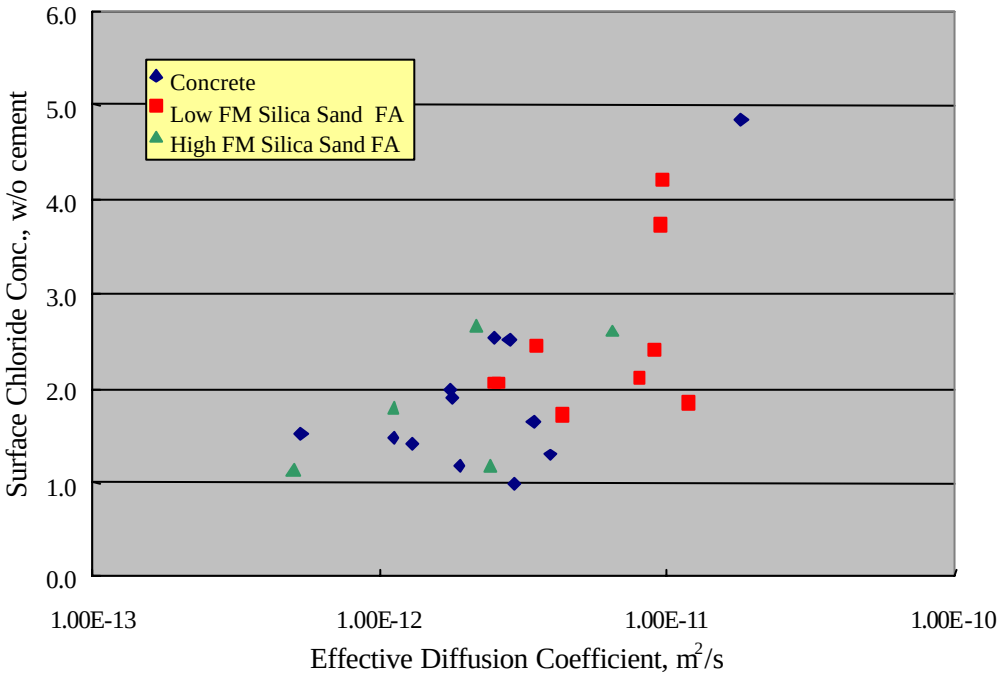

Figure 36: Plot of surface chloride concentration versus effective diffusion coefficient for mortar and concrete specimens.

ACKNOWLEDGEMENT

The authors express gratitude to Mr. George Jones for assistance with the experiments.

CONCLUSIONS

Mortar specimens with silica sand of either of two fineness moduli and concrete specimens were cyclically wet-dry ponded with a ten w/o NaCl solution for approximately one year. Mix design variables included 1) water-cement ratio (0.38, 0.45, and 0.52 (concrete specimens) or 0.55 (mortar specimens), 2) sand-cement ratio in the case of mortar specimens and fine aggregate-coarse aggregate-cement ratio for concrete ones, 3) coarse aggregate type (porous Florida limestone (SLF), dense Alabama limestone (VLA), and Ohio quartz (QO)), 4) coarse aggregate grading (as-received, which was not within specification, and rescreened and regraded (ideal), which was). The following conclusions were reached.

1. The effective chloride diffusion coefficient, D_{eff}, and the surface chloride concentration, c_s, are both important parameters that affect the rate of chloride ingress and occurrence of reinforcing steel corrosion and concrete cracking and spalling. Both parameters varied with mix design.

2. Surface chloride concentration and D_{eff} generally increased for the three specimen types in the following order: concrete, high fineness modulus silica sand mortar, and low fineness modulus silica sand mortar.

3. The D_{eff} of mortar specimens was relatively low for the two intermediate sand-cement ratios (0.5 and 1.0) and high for the two extremes (0 and 2.0). If this same trend applies to concretes as well, then the mortar portion within concretes may be of relatively high chloride permeability, since concretes are often designed with a sand-cement ratio of about two. This trend, where D_{eff} was relatively high at a sand-cement ratio of zero and two and low at 0.5 and one, suggests two competing processes where, first, interconnectivity of a relatively porous paste transition zone adjacent to aggregate particles, as has been reported from previous research, was increasingly important with increasing sand-cement ratio and dominated at the highest value (two) and, second, aggregate related chloride ingress impediment was controlling in the lower sand-cement ratio range.

4. The D_{eff} for specimens with water-cement ratio 0.38 was either about the same (mortar specimens) or higher (concrete specimens) than for a ratio of 0.45. This is thought to have resulted because a superplasticizer was not included in the mix design such that these materials were stiff and difficult to place. Specimens with water-cement ratio 0.52 (concrete) and 0.55 (mortar) invariably exhibited a higher D_{eff} than for a ratio of 0.45. On this basis, data for the 0.38 water-cement ratio specimens is considered suspect.

5. For concrete specimens with water-cement ratio 0.45, D_{eff} increased in proportion to the coarse aggregate-to-fine aggregate ratio, which was also in proportion to the volume fraction of coarse aggregate.

6. The surface chloride concentration for the present specimens was generally in the range 1.0-2.7 w/o cement (3-10 kg/m^3 of concrete or 0.13-0.45 on a w/o basis) in general agreement with the previously reported range.

7. The Iowa Pore Index for the SLF coarse aggregate was 208/44, whereas the Indices for the VLA and QO were 0/2 and 12/2, respectively. According to accepted interpretation of data from this test, the SLF aggregate had well interconnected macro- and capillary pores and should exhibit poor durability. The opposite is true for the VLA and QO aggregates.

8. Results from intrusion mercury porosimetry tests indicated that the SLF aggregate had the greatest cumulative concentration of pores and largest pore surface area. The VLA aggregate had the greatest cumulative pore volume and surface area for relatively large pores, but these parameters moderated in the capillary size range. Cumulative pore volume was lowest for the QO aggregate; however, its cumulative pore surface area was approximately the same as for the VLA. A disproportionate fraction of the QO material pore surface area was in the smallest pore size range (less than 0.01 μm diameter).

9. The D_{eff} for the concrete specimen fabricated using the SLF coarse aggregate was 16 and 26 percent higher than for the VLA and QO aggregates, respectively. This difference is considered modest in view of the highly porous nature of the SLF material and the fact that the QO is one of the densest aggregates in the United States. Apparently, coarse aggregate pore structure is not a significant factor where concrete durability and service life are controlled by chloride induced reinforcement corrosion. This finding suggests that the Iowa

Pore Index and mercury porosimetry results are not useful for qualifying or characterizing coarse aggregates for such service.

10. The relatively high c_s and D_{eff} values for the low fineness modulus mortar specimens compared to those for the high could have resulted from Cl^- absorption by some of the Ca-rich fine aggregate particles that were present. Alternatively, the smaller fine aggregate particles may have provided less of an impediment to Cl^- diffusion than the larger ones.

11. Grading of the as-received high fineness modulus fine aggregate and the as-received SLF coarse aggregate did not conform to specification in that the particle size range in both cases was too narrow with an absence of larger size particles. Concrete specimens fabricated using these aggregates resulted in a higher D_{eff} than ones for which the coarse aggregate was rescreened and then regraded to within specification. For a water-cement ratio of 0.45, this difference was by 16 percent.

12. The finding that aggregate grading did not conform to specification is thought to have resulted from the materials handling procedure which involves the following steps:

    a. Upon mining and crushing, the stone is separated into nine stockpiles according to size.

    b. The stone from these piles is then batched (blended) according to the specific job specification.

    c. The resultant CA is then loaded into a rail car and transported to a concrete plant.

    d. Upon arrival at the concrete plant, the aggregate is bottom dumped into a silo. This results in an inverted cone with finer particles at the center and coarser at the outside.

    e. The aggregate is transported upon a conveyer belt to the mixer. Both FDOT and plant inspectors check the gradation every two-three months by taking three samplings from the belt at three different times, mixing these, and sieving.

    The potential short-coming of this method is that the aggregate is segregated on the belt but may be re-proportioned to within specification when the three segregated samples are mixed. Consequently, the quality control procedure may be flawed.

13. Scanning electron microscopy and energy dispersive x-ray analysis of cores acquired from the chloride exposed specimens indicated that concentration of this species (chlorides) in the

SLF coarse aggregate and high fineness modulus silica sand fine aggregate was below the detection limit of the instrumentation. Chlorides were detected in the low fineness modulus sand particles that were Ca-rich. This confirms the previous projection that chlorides migrate through the cement paste only with the aggregates serving as an impediment to this transport and is consistent with the finding that, first, D_{eff} for specimens of each of the three coarse aggregate types was generally the same and, second, some D_{eff} reduction was affected by specification compared to non-specification graded coarse aggregate.

RECOMMENDATIONS

Based upon the results of this research, the following are recommended:

1. A statistically significant survey of fine and coarse aggregate grading that is being realized in Florida bridge construction should be performed. This could be accomplished by sampling fresh concrete at construction sites about the State, washing the material, and screening. By comparison of these gradings with results of this research, it should be possible to estimate the D_{eff} improvement that could be realized if the aggregate grading was within specification.

2. It was determined that chlorides were present in the Ca-rich fine aggregate particles, whereas this species was absent in the coarse aggregate. Apparently, the propensity for chlorides to be present in Florida limestone aggregates is size dependent. The size or size range at with this transition occurs should be determined.

3. Studies of mix design improvements that can be affected based upon fine and coarse aggregate gradings should be continued.

BIBLIOGRAPHY

1. Hausmann, D.A., *Materials Protection*, Vol. 6(10), 1967, p. 23.
2. Gouda, V.K., *British Corrosion Journal*, Vol. 5, 1970, p. 198.
3. Hausmann, D.A., *Materials Performance*, Vol. 37(10), 1998, p. 64.
4. Breit, W., *Mater. Corrosion*, Vol. 49, 1998, p. 539.

5. Charvin, S., Hartt, W.H., and Lee, S. K., "Influence of Permeability Reducing and Corrosion Inhibiting Admixtures in concrete upon Initiation of Salt Induced Embedded Steel Corrosion," paper no. 00802 presented at CORROSION/00, March 26-31, 2000, Orlando.

6. Li, L. and Sagüés, A.A., *Corrosion*, Vol. 57, 2001, p. 19.

7. Glass, G.K. and Buenfeld, N.R., "Chloride Threshold Levels for Corrosion Induced Deterioration of Steel in Concrete," paper no. 3 presented at RILEM International Workshop on Chloride penetration into Concrete, Oct. 15-18, 1995, Saint Rémy-les-Chevreuse.

8. Tutti, K., *Corrosion of Steel in Concrete*, Report No. Fo 4, Swedish Cement and Concrete Research Institute, Stockholm, 1982.

9. Bamforth, P.B., "Definition of Exposure Classes and Concrete Mix Requirements for Chloride Contaminated Environments," *Corrosion of Reinforcement in Concrete*, Eds: Page, C.L., Treadaway, K.W.J., and Bamforth, P.B., Soc. Chem. Ind., London, 1996, p. 176.

10. Bamforth, P.B. and Price, W.F., "Factors Influencing Chloride Ingress into Marine Structures," *Concrete 2000*, Eds: Dhir, R.K. and Jones, M.R., E&FN Spon, London, 1993, p. 1105.

11. Thompson, N.G. and Lankard, D.L., "Improved Concretes for Corrosion Resistance," Report No. FHWA-RD-96-207, Federal Highway Administration, 1997.

12. "Specification for Concrete Aggregates," ASTMC33-01, *Annual Book of Standards*, American Society for Testing and Materials, 100 Barr Harbor Drive, West Conshohocken, PA 19428.

13. "Florida Method of Test for Determining Low-Levels of Chloride in Concrete and Raw Materials," Designation FM 5-516, Florida Department of Transportation, Tallahassee, FL, Sept., 1994.

14. Mr. Jerry Haught, Rinker Materials Corporation, West Palm Beach, FL, personal communication.

15. Eades, J.L., McClellan, G.H., and Fountain, K.B., "Evaluation of Soundness Tests on Florida Aggregates", Final Report, FDOT Contract B-8354 (WPI 0510682), March, 1997.

16. Bamforth, P.B. and Pocock, D.C., "Minimizing the Risk of Chloride Induced Corrosion by Selection of Concreting Materials," *Corrosion of Reinforcement in Concrete*, Ed: Page, C.L., Treadaway, K.W.J., and Bamforth, P.B., Soc. Chemical Ind., London, 1990.

17. Diederichs, V., Hinrichsmeyer, K., and Schneider, U., "Analysis of Thermal, Hydrothermal, and Mechanical Stresses of Concrete by Mercury-Porosimetry and Nitrogen-Sorption," Proceedings, RILEM/CNR International Symposium of *Principles and Applications of Pore Structural Characterization*, Milan, April, 1983.

18. Winslow, D.N., The Pore Structure and Surface Area of Hydrated Portland Cement Paste," in Characterization *and Performance Prediction of Cement and Concrete*, Ed. J.F. Young, Engr. Foundation, New York, 1984, p. 105.

19. Winslow, D.N. and Liu, D., *Cement and Concrete Research*, Vol. 20, 1990, p. 227.

20. Winslow, D.N. Cohen, M.D., Bentz, D.P., Snyder, K.A., and Garboczi, E.J.., *Cement and Concrete Research*, Vol. 24, 1994, p. 25.

21. Halamickova, P., Detwiler, R.J., Bentz, D.P., and Garboczi, E.J., *Cement and Concrete Research*, Vol. 25, 1995, p. 790.

22. Young, J.F., "A Review of the Pore Structure of Cement Paste and Concrete and Its Influence on Permeability," in *Permeability of Concrete*, Eds. D. Whiting and A. Walitt, ACI SP-108, American Concrete Institute, 1988, p. 1.

23. Andrade, C., Sanjuán, M.A., Recuero, A., and Río, O., *Cement and Concrete Research*, Vol. 24, 1994, p. 1214.

24. Maso, J. C., "The Bond between Aggregates and Hydrated Cement Pastes," Proceedings, Seventh International Conference on the *Chemistry of Cement*, Vol. 1, Paris, 1980, p. VII-1.